

**THERMAL ENERGY STORAGE USING PARAFFIN WAX AND STABILITY
STUDY OF THE PHASE CHANGE MATERIAL CONTAINING
NANOPARTICLES**

by Vahit Saydam

A thesis submitted to the School of Graduate Studies
in partial fulfillment of the requirements for the degree of

Master of Engineering

Faculty of Engineering & Applied Science

Memorial University of Newfoundland

May 2018

St. John's Newfoundland and Labrador

Abstract

This thesis has two main parts. In the first part, the performance of a helical coil heat exchanger was investigated with paraffin wax as the phase change material (PCM) for a latent heat thermal energy storage system (LHTESS). The effects of heat transfer fluid (HTF) inlet temperature, HTF flow rate and flow direction were experimentally examined by measuring PCM temperature changes in the charging and discharging processes. The experimental results showed that HTF inlet temperature has the greatest influence on the charging/discharging processes. The flow direction of HTF had only an insignificant effect on discharging time. Higher heat recovery efficiency was achieved at high flow rates during discharging. Overall, it was seen that the low thermal conductivity of paraffin wax led to poor heat transfer performance, specifically causing much longer discharging times compared to charging times.

In the second part of the thesis, nanoparticle-enhanced phase change materials (NEPCMs) were proposed as a heat transfer enhancement method. Various highly conductive nanoparticles were dispersed into paraffin wax to improve the thermal conductivity of the PCM. Multi-walled carbon nanotubes (MWCNTs), graphene nanoplatelets (GNPs) and Aluminum oxide (Al_2O_3) nanoparticles were selected as enhancers. Nanoparticles were dispersed into paraffin wax using mechanical dispersion methods (sonication, stirring) with and without surfactants at varying mass fractions (0.1, 0.5, 1 and, 2 wt.%). The stability of nanoparticles was investigated after consecutive melting/solidification cycles were performed in an environmental chamber. Significant deposition and coagulation were seen over thermal cycles regardless of the nanoparticle type, nanoparticle content and dispersion

method. The presence of nanoparticles did not lead to the desired thermal conductivity enhancement due to particle deposition and stability issues. The highest thermal conductivity enhancement was achieved by 13% for a 2 wt.% MWCNT-wax sample at 35°C. Differential Scanning Calorimetry (DSC) measurements also showed an insignificant change in latent heat capacity. In conclusion, NEPCMs could be an alternative storage material for LHTESS to improve overall heat transfer performance only if the issues associated with particle stability are resolved. Therefore, further study regarding the stability of NEPCMs with a multidisciplinary approach is needed to solve this problem.

Acknowledgements

I would like to thank my supervisor, Dr. Xili Duan, for providing me the opportunity to join his research team. This thesis would not have been possible without his help and support throughout my research. All our fruitful discussions and his guidance played a key role in dealing with the challenging aspects of this study. My colleague, Mohammad Parsazadeh, also has my gratitude for sharing his valuable opinions and insight on the subject and helping me cope with the issues I faced during my study. I also would like to thank Dr. Helen Zhang and her students for allowing me to use the equipment in their lab. I acknowledge the financial support provided by the Natural Sciences and Engineering Research Council of Canada (NSERC) and NL Innovation Council. I also acknowledge the funding granted by the School of Graduate Studies (SGS) at Memorial University of Newfoundland.

Finally, I am grateful to my family for their unending love and constant support in bad and good times. Hence, I dedicate this thesis to them.

Contents

Abstract	i
Acknowledgements	iii
List of Tables	vi
List of Figures	vii
List of Abbreviations and Symbols.....	x
Chapter 1 Introduction	1
1.1 Background	1
1.2 Research Objectives	4
1.3 Outline of Thesis	4
Chapter 2 Literature Review	6
2.1 Latent Heat Thermal Energy Storage.....	6
2.2 Nano-Enhanced Phase Change Materials	10
2.2.1 Characterization and thermal property of the enhancement of NEPCM	11
2.2.2 Stability of NEPCM.....	16
2.3 Literature Summary.....	30
Chapter 3 Experimental Research on LHTESS with Paraffin Wax as a PCM.....	32
3.1 PCM Heat Exchanger and Experimental Setup	32
3.1.1 Theoretical design of the thermal energy storage unit.....	32
3.1.2 Design and fabrication of the helical coil heat exchanger thermal energy storage unit	33
3.1.3 Experimental setup.....	35
3.2 Experimental Results and Discussions.....	37
3.2.1 Charging.....	39
3.2.2 Discharging	40
3.2.3 The effect of the HTF volume flow rate	43
3.2.4 The effect of HTF inlet temperature on charging	46
3.2.5 The effect of the HTF flow direction	47
3.2.6 Storage efficiency	49
3.3 Summary	50
Chapter 4 Characterization and Stability Study of NEPCM.....	51

4.1 Materials and Methods	51
4.1.1 Materials	51
4.1.2 Sample preparation	52
4.2 Thermal Conductivity Measurements	53
4.2.1 Monitoring the thermal conductivity of NEPCMs in liquid phase	55
4.2.2 Thermal conductivity change of NEPCMs with temperature	57
4.3 Differential Scanning Calorimetry (DSC) Measurements	61
4.4 Stability of Paraffin Wax with Nanoparticles	64
4.4.1 Effect of sonication on the stability of mechanically-prepared NEPCM	64
4.4.2 Effectiveness of surfactants on the stability of NEPCM.....	67
4.4.3 Effect of boundary conditions on stability	70
4.5 Summary	71
Chapter 5 Conclusions and Recommendations.....	73
5.1 Conclusions for Experimental Study of LHTESS with Paraffin Wax	73
5.2 Conclusions for NEPCM Study with Paraffin Wax.....	74
5.3 Recommendations for Future Work	75
References	76

List of Tables

Table 2.1: Summary of PCM type, nanoparticle type, size and fraction	21
Table 2.2: Summary of preparation, characterization, heat transfer study and stability of NEPCM.....	24
Table 3.1: Properties of PCM and HTF (Ukrainczyk et al., 2010)	33
Table 3.2: Outline of the experiments under different operational conditions	38
Table 4.1: DSC results of NEPCM samples ($T_{m,peak}$: peak melting temperature, $T_{s,peak}$: peak solidification temperature, ΔT : supercooling, ΔH_m : enthalpy of solid-liquid transition during melting, ΔH_s : enthalpy of solid-liquid transition during solidification).....	62

List of Figures

Figure 3.1: Fabrication of the heat exchanger and the storage tank.	35
Figure 3.2: (a) Schematic of the experimental setup; (b) Positions of thermocouples; T1: Side bottom, T2: Center bottom, T3: Center middle, T4: Center top, T5: HTF inlet, T6: HTF outlet.	37
Figure 3.3: Comparison of charging and discharging times at different operational conditions.	38
Figure 3.4: Charging with a flow rate of 4 LPM at a 75°C HTF inlet temperature.	40
Figure 3.5: Pictures of charging with a flow rate of 4 LPM at 75°C (A: 30 min, B: 60 min, C: 90 min, D: 120 min, E: 145 min, F: 170 min).	41
Figure 3.6: Discharging with a flow rate of 1 LPM at a 20°C HTF inlet temperature.	42
Figure 3.7: Pictures of discharging test with a flow rate of 1 LPM at 20°C (A: 0 min, B: 30 min, C: 150 min).	42
Figure 3.8: Temperature profile of the center top thermocouple at different flow rates during charging at 75°C.	43
Figure 3.9: Temperature profile of the center bottom thermocouple at different flow rates during charging at 75°C.	44
Figure 3.10: Temperature profile of the center top thermocouple at different flow rates during discharging at 20°C	45
Figure 3.11: Temperature profile of the center top thermocouple at different HTF inlet temperatures with 4 LPM during charging.	46

Figure 3.12: Temperature profile of the center bottom thermocouple at different flow directions with 4 LPM during charging at 75°C.....	47
Figure 3.13: Temperature profile of the center bottom thermocouple at different inlet positions with 1 LPM during discharging at 20°C.....	48
Figure 4.1: A: Paraffin wax, B: MWCNTs, C: Al ₂ O ₃ , D: GNPs. E: Sodium oleate, F: Octadecylamine.....	52
Figure 4.2: Sample preparation using the mechanical dispersion method.....	52
Figure 4.3: KD2 Pro Thermal Conductivity Analyzer and its sensors: TR-1, KS-1, SH-1 (from left to right).	55
Figure 4.4: Thermal conductivity change in liquid phase (60°C) over time after sample preparation.	56
Figure 4.5: 3-D printed mold for thermal conductivity measurements in solid phase.....	57
Figure 4.6: Picture of each sample after being removed from the mold.....	57
Figure 4.7: Thermal conductivity change of MWCNT-wax samples with temperature. ..	59
Figure 4.8: Thermal conductivity change of GNP-wax samples with temperature.....	59
Figure 4.9: Thermal conductivity change of Al ₂ O ₃ -wax samples with temperature.	60
Figure 4.10: Mettler-Toledo DSC1, Differential Scanning Calorimeter.	63
Figure 4.11: DSC heating and cooling curves of paraffin wax with MWCNT, GNP and Al ₂ O ₃ nanoparticles at different concentrations.....	63
Figure 4.12: Stability observation of MWCNT-wax samples in liquid phase over first (1), second (2) and, third (3) melting/solidification cycles (Sample A: 0.1 wt.%, 100 min sonication; B: 0.1 wt.%, 40 min sonication; C: 0.075 wt.%, 70 min sonication, D: 0.05 wt.%, 100 min sonication, E: 0.05 wt.%, 40 min sonication).....	66

Figure 4.13: Settling of MWCNTs in paraffin wax.....	66
Figure 4.14: Stability observation of different types of nanoparticles in paraffin wax with sodium oleate as a surfactant in NEPCM preparation, #C represents the number of melting/solidification cycles.	67
Figure 4.15: Stability observation of various NEPCM prepared with octadecylamine.....	69
Figure 4.16: Solidification of a 0.01wt.% MWCNT-wax sample after melting on a hot plate at 150°C.	71

List of Abbreviations and Symbols

η	Recovery efficiency of the storage unit
ΔH_m	Enthalpy of solid-liquid transition during melting
ΔH_s :	Enthalpy of solid-liquid transition during solidification
AcCOOH	Glacial acetic acid
AFM	Atomic force microscope
Ag	Silver
Al ₂ O ₃	Aluminum oxide
Au	Gold
C-S-WCNT	Carboxyl-functionalized short-multi-walled carbon nanotubes
CMC	Critical micelle concentration
CNF	Carbon nanofibers
CNT	Carbon nanotubes
CNW	Carbon nanowires
$C_{p,HTF}$	Specific heat of heat transfer fluid
$C_{p,pcm,l}$	Specific heat of the wax at liquid phase
$C_{p,pcm,s}$	Specific heat of the wax at solid phase
CTAB	Cetyl trimethylammonium bromide
Cu	Copper
CuO	Copper oxide
DAQ	Data acquisition system
DLS	Dynamic light scattering
DSC	Differential scanning calorimeter
EG	Ethylene glycol
f-MWCNT	Functionalized multi-walled carbon nanotubes
FTIR	Fourier transform infrared spectroscopy
G-MWCNT	Graphitized multi-walled carbon nanotubes

GNP	Graphene nanoplatelets
H_{pcm}	Latent heat capacity of paraffin wax
k_{pcm}	Thermal conductivity of paraffin wax
L-MWCNT	Long- multi-walled carbon nanotubes
LHS	Latent heat storage
LHTESS	Latent heat thermal energy storage system
LPM	Liter per minute
\dot{m}_{HTF}	Mass flow rate of heat transfer fluid
MWCNT	Multi-walled carbon nanotubes
NEPCM	Nano-enhanced phase change materials
Nm	Nanometers
PC	Personal computer
PCM	Phase change materials
PEG	Polyethylene glycol
Rpm	Revolution per minute
PVA	Polyvinyl alcohol
S-MWCNT	Short-multi-walled carbon nanotubes
SA	Salicylic acid
SDS	Sodium dodecyl sulfate
SEM	Scanning electron microscope
SHS	Sensible heat storage
TEA	Triethylamine
TEM	Transmission electron microscope
TEMED	Tetraacetylenediamine
THW	Transient hot wire method
TPS	Transient plane source method
TSHW	Transient-short-hot-wire method

T_f	Final temperature of the wax
T_i	Initial temperature of the wax
T_{in}	Inlet HTF temperature
T_m	Melting temperature of the wax
T_o	Outlet HTF temperature
$T_{s,peak}$	Peak solidification temperature
$T_{m,peak}$	Peak melting temperature
UV-Vis	Ultraviolet-visible spectroscopy
xGNP	Exfoliated graphene nanoplatelets
XRD	X-ray diffraction

Chapter 1 Introduction

This thesis consists of two parts. In the first part, experimental analysis of a latent heat thermal energy storage system (LHTESS) was conducted. Experimental results revealed that the inherent low thermal conductivity of paraffin wax affected the charging and discharging performance of LHTESS. In the second part, various nanoparticles were dispersed into paraffin wax to improve its thermal conductivity. The thermal conductivity improvement and stability of the nanoparticles in wax were investigated in detail.

1.1 Background

The growing population and world economy are consuming more energy than ever. Increasing energy production is heavily dependent on fossil fuels, which have adverse effects on the environment. To keep up with this ever-increasing demand, widespread efforts have been made to use sustainable energy sources more efficiently. Clean energy sources such as wind and solar have great potential in energy production. However, the intermittency and inconsistency associated with these energy sources raise questions about their reliability and availability, since a constant supply of energy is needed, particularly at peak times. Therefore, storing renewable energy for later use when it is available plays a key role in the shift from fossil fuels to renewable energy, paving the way for a cleaner and brighter future for future generations.

Among the various energy storage methods, thermal energy storage is one of the most widely-implemented storage methods (Dincer & Rosen, 2002). The abundance of energy sources such as solar, geothermal energy and waste heat generation in residential and industrial applications provide a strong motivation for harnessing these types of energy

sources. Apart from chemically-stored thermal energy, there are two thermal energy storage methods. Sensible heat storage (SHS) is based on the principle of storing energy by increasing the temperature of the storage material. Water and rock are common materials that have been used for this purpose for centuries (Huggins, 2010). The other method that makes use of the phase change of the storage materials is latent heat storage (LHS). A significant amount of energy is released or absorbed when phase change (solid-liquid, liquid-gas) takes place at a constant temperature. LHS has a few advantages over SHS such as higher energy density and regulatory features by preventing temperature fluctuations, particularly in domestic hot water applications (Mehling & Cabeza, 2007; Barreneche et al., 2015).

Latent heat storage materials are called phase change materials (PCMs). PCMs are divided into two main categories: organic and inorganic PCMs. Organic PCMs consist of paraffin compounds (alkanes) and fatty acids. The availability at moderate temperatures (0-100 °C) makes organic PCMs the best candidate for the thermal management of electronic devices, residential air conditioning and domestic hot water applications (Fleischer, 2015; Sharma et al., 2009). Organic PCMs have many desirable features including low cost, chemical stability and non-toxicity. Moderately high heat of fusion and minor super-cooling are other favorable properties that have drawn a lot of attention to the use of organic PCMs in cyclic thermal storage applications (Pelichowska & Pielichowski, 2014). That said, there is one drawback that affects the performance of storage efficiency during charging and discharging: the low thermal conductivity of these PCMs (0.15-0.3 W/m·K) (Dincer & Rosen, 2002; Farid et al., 2004). Inorganic PCMs, however, have higher thermal conductivity (0.6- 0.7 W/m·K) and include mostly salt hydrates. Salt hydrates tend to melt

incongruently and experience phase segregation. In addition, the high level of supercooling stemming from poor nucleation causes freezing at lower temperatures and energy loss (Hyun et al., 2014; Kenisarin & Mahkamov, 2007).

Types of thermal energy storage that take advantage of the high latent heat of PCMs have been used extensively. Despite having low thermal conductivity, paraffin wax stands out among other types of PCMs in LHTESS applications because of its favorable properties mentioned above. Several methods have been tested to enhance the thermal conductivity of paraffin compounds. Some of the previous efforts have involved inserting metallic fins and matrix structures into PCMs (Kenisarin & Mahkamov, 2007; Xu et al., 2015). In recent years, there has been growing interest in dispersing highly conductive nano-sized particles into PCMs for thermal conductivity enhancement. Nanoparticles could help PCMs overcome some of their deficiencies such as low thermal conductivity and poor nucleation (Khodadadi et al., 2013). So far, most studies of nano-enhanced phase change materials (NEPCMs) have focused on the change in thermal conductivity, latent heat and viscosity with the presence of nanoparticles. The consensus is that the addition of nanoparticles yields an increase in thermal conductivity at varying degrees. Even so, this improvement has unpleasant consequences such as a reduction in latent heat capacity and a dramatic increase in viscosity (Kibria et al., 2015). These outcomes are the cause of less energy being stored and suppressed natural convection affecting the charging time for LHTESS.

1.2 Research Objectives

This study focuses on the two different aspects of LHTESS. The first aspect deals with the experimental analysis of LHTESS. The scope of this first part can be summarized as follows:

- 1) Observing the solidification and melting characteristics of paraffin wax in a helical coil embedded heat exchanger for latent heat thermal energy storage.
- 2) Conducting sensitivity analysis by changing the operational parameters. The flow rate, the flow direction and inlet temperature of the heat transfer fluid are varied to examine the effects on charging and discharging time.

The second part, which deals with using NEPCMs as a heat transfer enhancement method for LHTESS, includes the following objectives:

- 3) Looking at the preparation and characterization of paraffin wax with various nanoparticles.
- 4) Studying the effect of dispersion methods on the stability of NEPCMs.

1.3 Outline of Thesis

The rest of the thesis can be summarized for each chapter as below:

- Chapter 2 provides a literature review on experimental studies of LHTESS with PCM and the characterization of NEPCMs.
- Chapter 3 is dedicated to the experimental work on LHTESS. The effects of operational conditions (HTF flow rate, HTF inlet temperature, flow direction of HTF) on the charging and discharging were studied.

- Chapter 4 describes the preparation, characterization and stability of NEPCMs using paraffin wax with various nanoparticles.
- Chapter 5 summarizes the main results of the study and gives recommendations for future research.

Chapter 2 Literature Review

In this chapter, existing experimental studies on latent heat thermal energy storage with phase change materials were reviewed. In addition, previous research efforts related to the current study addressing the characterization and stability of NEPCM were also briefly summarized.

2.1 Latent Heat Thermal Energy Storage

Energy supply from many sustainable sources, such as solar, thermal or wind, is intermittent in nature, and there is often a time lag between supply and demand. Therefore, efficient energy storage is critical for practical applications of these sustainable energy sources (Chu & Majumdar, 2012). For residential solar thermal applications, conventional hot water systems have relatively low efficiency and limited capacity, particularly at night and during days without sunshine. To overcome these problems, PCMs have been used to store thermal energy (Akgün et al., 2008; Zhou & Zhao, 2011; Sarı & Karaipekli, 2007). PCMs have advantageous features such as nearly isothermal solid-liquid phase change and a high energy storage capacity due to the latent heat of fusion. Latent heat storage systems, when compared to sensible heat storage systems, have a significantly higher energy density, leading to fewer storage materials, or smaller volumes needed to yield the same amount of energy for a sensible heat storage system (Fleischer, 2015).

There have been many different types of phase change thermal energy storage systems studied in the literature (Al-Abidi et al., 2016; Nomura et al., 2013; Dutil et al., 2011). These studies involved various storage geometries with heat exchanger configurations. For higher efficiency and more compact design of the storage system, a higher heat transfer

rate between the heat transfer fluid and PCM is desired. Therefore, the heat exchanger type plays a crucial role in the design of thermal storage units. Maximized contact area between the PCM and heat exchanger surface is required due to the poor heat transfer performance of the PCM. Another factor to be considered in the design is the pressure drop developed from frictional losses through the heat exchanger. The optimal design will aim to limit the local pressure drop while not compromising the device's performance. Among the several heat exchanger designs, the helical coil configuration stands out due to the increased heat transfer surface area. Therefore, some of the researchers chose to use a helical coil design in their studies (Huang et al., 2011; Kabbara et al., 2014; Korti & Tlemsani, 2016; Sundaram et al., 2016; Dinker et al., 2016; Tayssir et al., 2016; Zhang et al., 2017; Yang et al., 2017).

The types of experimental setups vary depending on the energy sources. The majority of experimental studies used thermal baths to provide the desired operational conditions (Korti & Tlemsani, 2016; Dinker et al., 2016; Tayssir et al., 2016; Zhang et al., 2017). Yet, other studies utilized solar energy through solar panels to perform real-time charging/discharging tests (Kabbara et al., 2014; Yang et al., 2017). Thermocouples are usually placed in the storage unit at various locations and data are recorded through data acquisition (DAQ) systems. In terms of the geometry of the storage unit, vertical cylindrical containers are widely preferred (Huang et al., 2011; Kabbara et al., 2014; Korti & Tlemsani, 2016; Dinker et al., 2016; Tayssir et al., 2016; Zhang et al., 2017; Yang et al., 2017). There are also studies that have used horizontal cylindrical (Sundaram et al., 2016) and rectangular containers (Dinker et al., 2017).

A few main operational factors can be varied to improve the performance of the thermal storage unit and its storage capacity. These factors are related to properties of the HTF, namely, the HTF inlet temperature and HTF flow rate. Most of the experimental studies proved that increasing the HTF inlet temperature results in reduced melting times at varying degrees (Korti & Tlemsani, 2016; Dinker et al., 2016; Tayssir et al.; 2016; Zhang et al., 2017; Yang et al., 2017). An increased temperature difference between HTF and PCM gives rise to a higher heat transfer rate. Yet, there is a limit in the reduction of charging times as discussed by Yang et al. (2017). They pointed out that increasing the inlet HTF temperature from 72°C to 77°C did not yield the same reduction in charging speed compared to a case where the inlet HTF temperature was increased from 67°C to 72°C. Charging at a low HTF inlet temperature was found to be more uniform throughout the storage, whereas charging at a high temperature induced more uneven dynamic melting (Korti & Tlemsani, 2016, Sundaram et al., 2016). The effect of the volumetric flow rate of HTF on charging and discharging, on the other hand, was found to be subtle (Zhang et al., 2017; Korti & Tlemsani, 2016, Sundaram et al., 2016) and sometimes negligible (Yang et al., 2017). This was because an increase in flow rate only enhances forced convection in the heat exchanger pipe; while an increase in HTF temperature improves the heat transfer among the HTF, heat exchanger and PCM (Yang et al., 2017). Tayssir et al. (2016) also showed the greater influence of the HTF flow rate on charging at high inlet HTF temperatures.

The prevailing heat transfer mechanism differs for charging and discharging. From the start of charging until gravity effects take over, conduction is the main means of heat transfer.

However, with the involvement of gravity effects, natural convection dominates the charging process. This behavior was shown by the deformation of the axisymmetric manner of melting in the further stages of charging (Korti & Tlemsani, 2016; Sundaram et al., 2016). Throughout solidification, however, the main heat transfer mechanism has been shown to be conduction (Ettouney et al., 2004 (July); Dinker et al., 2016). Kabbara et al (2014) showed that the discharging times were much longer than the charging times due to the conduction-dominated heat transfer process within dodecanoic acid, which has a low thermal conductivity. Huang et al. (2011) also found that increasing a microencapsulated PCM slurry concentration resulted in the suppression of natural convection during melting. This was attributed to the higher density and low thermal conductivity of slurry, deteriorating the heat transfer between the heat exchanger and storage material.

Despite the high storage capacity of PCMs, low thermal conductivity limits the performance of thermal storage units. Thus, heat transfer enhancement methods are indispensable to reduce charging/discharging times. Traditional methods including using extended fins, metallic structures and matrixes were summarized in some of the review papers (Kenisarin & Mahkamov, 2007; Fan & Khodadadi, 2011; Xu et al., 2015). Ettouney et al., 2004 (November) pointed out that using metal spheres as enhancers accelerated the melting process by three times, although the presence of metal spheres decreased the storage capacity by less than 2%. Fins and metal matrices were found to be very effective in increasing the heat transfer rate, particularly during solidification. However, using fins as enhancers comes at a price. The excessive usage of fins depending on the geometry could deteriorate natural convection effects as well as reduce the storage capacity. Agyenim et al.

(2009) showed that circular fins in a concentric tube storage setup degraded the heat transfer rate during melting.

2.2 Nano-Enhanced Phase Change Materials

The idea of using nanoparticles as enhancers goes back to 1995, when Dr. Choi summarized the potential of nanoparticles in the thermal property enhancement of heat transfer fluids and coined the term “Nanofluid” (Choi & Eastman, 1995). Nanoparticles are referred to particles with a size range of 1 to 100 nanometers (nm) (Michaelides, 2014). They differ from bulk materials because of their unique electrical, chemical and thermal properties. There are various types of nanoparticles being used as enhancers for PCMs including carbon-based nanoparticles such as multi-walled carbon nanotubes (MWCNTs), carbon nanofibers (CNFs), carbon nanowires (CNWs), graphene nanoplatelets (GNPs), graphite and metal and metallic oxide nanoparticles like Copper (Cu), Silver (Ag), Gold (Au), Aluminum Oxide (Al_2O_3) and Copper Oxide (CuO) (Das et al., 2007).

After almost a decade, the novel idea of the addition of nanoparticles for the thermal property enhancement of PCMs was gradually put in place and NEPCMs were devised (Khodadadi & Hosseinzadeh, 2007). Since then, there have been numerous studies incorporating nanoparticles into base PCMs. The main scope is to improve thermal conductivity and analyze other properties including viscosity, latent heat, melting temperature, etc. NEPCM studies have shown promising results in terms of thermal conductivity improvement. Other properties, however, have been degraded to varying extents. For instance, the level of viscosity increase or latent heat capacity reduction with

the presence of nanoparticles in PCMs raises the question of the feasibility of NEPCMs. Therefore, the benefits of utilizing nanoparticles still need to be justified.

This section mainly covers the summary of previous studies focusing on the characterization and heat transfer enhancements of paraffin compounds with different nanoparticles. Reviewed papers were mostly chosen based on PCM type, which is paraffin compounds (alkanes). Carbon-based nanofillers (MWCNT, CNT, and GNP) and Al_2O_3 dispersed paraffin wax were given extra emphasis. Sample preparation techniques and characterization methods of nanocomposites were elaborated. Thermal conductivity enhancement and stability observation constitute the primary focus of the papers reviewed. Furthermore, the details of PCM, nanoparticle type, size and fraction were summarized in Table 2.1. Sample preparation methods, methods and instruments for characterization and stability information, if included in the study, were provided in Table 2.2.

2.2.1 Characterization and thermal property of the enhancement of NEPCM

As described above, this part of the literature review centers on NEPCMs' preparation, characterization methods, and thermal property enhancement. The effects of various nanoparticles on the thermal properties of PCMs, specifically thermal conductivity, were scrutinized.

NEPCMs can be prepared with several methods, including mechanical and chemical dispersion methods. Mechanical dispersion methods include stirring (shear mixing) and sonication. Stirring helps nanoparticles disperse at a macro scale by spinning a stirring bar in the liquid medium. During sonication, cavitation is generated in the liquid in which micro bubbles form and collapse suddenly, leading to a good dispersion (Branson Ultrasonics

Corporation, 2001). The significant amount of energy provided to the solution may decrease the aspect ratio of the MWCNT and have a detrimental effect on their conductive properties (Sabet et al., 2015). Therefore, it is important to find the optimal sonication energy level and time in the preparation of the NEPCMs. Another widely-used dispersion method is the use of surfactants, which is a chemical method. Surfactants help nanoparticles disperse better by altering the surface energy levels to make them less prone to agglomeration. However, the addition of surfactants can also change the thermal properties of the nanoparticles (Kamalgharibi et al., 2016).

The researchers' choice of dispersion method in their studies varies widely depending on the nanoparticle type and base PCM (Table 2.1). The studies implementing mechanical dispersion usually follow the sequence of stirring (shear mixing) and sonication of nanoparticles at differing durations in liquid-based PCMs (Shaikh et al., 2008; Teng & Yu, 2012; Yu et al., 2013; Fan et al., 2013; Fang et al., 2013; Zeng et al., 2013; Yang et al., 2014; Wu et al., 2016; Lokesh et al., 2015). There are exceptions as well where only stirring (Elgafy & Lafdi, 2005; Kim & Drzal, 2009) or sonication (Weinstein et al., 2008; Warzoha & Fleischer, 2014; Jesumathy et al., 2012) is used for the dispersion of nanoparticles. Some researchers also preferred using surfactants such as octadecylamine (Tang et al., 2014), sodium oleate (Fan & Khodadadi, 2011(March); Nabil & Khodadadi, 2013), oleylamine (Wang et al., 2010) along with stirring and sonication for the surface modification of nanoparticles to make them more dispersible in base PCMs. Other stabilization and preparation methods include acid treatment (Zhang et al., 2012; Mehrali et al., 2013;

Angayarkanni & Philip, 2015), functionalization (Tang et al., 2014) and exfoliation processes for xGNPs (Kim and Drzal, 2009).

The most important area of study regarding NEPCM characterization is thermal conductivity enhancement. MWCNTs, which are some of the most commonly used nanoparticles, have been shown to result in thermal conductivity enhancement, but sometimes with contradicting results. Warzoha and Fleischer (2014) claimed abnormal improvement reaching up to 2.5 W/m·K at high loadings (20 vol.%) of MWCNT in wax, while Angayarkanni and Philip (2015, June) showed that thermal conductivity was improved by 195% for a 0.05 wt.% MWCNT-wax composite. They pointed out that the reduced interfacial thermal resistance, internal stress and percolated network of nanoparticles at low loadings contributed to an improvement in thermal conductivity. Some researchers also pointed out a moderate improvement in thermal conductivity by at most 50% with the presence of MWCNTs at different loadings (Wang et al., 2009; Kumaresan et al., 2012; Cui et al., 2011). On the other hand, other researchers indicated only insignificant enhancement up to 20% (Yu et al., 2013; Fan et al., 2013). Wu et al. (2016) even stated no improvement with the dispersion of MWCNTs in paraffin wax at 0.5 - 3 wt. %. A highly entangled and prone to agglomeration structure was held accountable for the poor performance of MWCNTs.

Dispersing another carbon-based nanoparticle, GNPs, have shown promising results in enhancing the thermal conductivity of paraffin wax. Kim and Drzal (2009) reported a remarkable increase from 0.229 W/m K to 0.8 W/m K for a 7 wt.% Paraffin/xGNP composite. Shi et al. (2013) showed that despite graphene's high thermal conductivity,

xGNP outweighed the performance of GNPs in enhancing thermal conductivity. This was attributed to smaller-sized graphene layers affecting the phonon boundary scattering adversely. Fan et al. (2014) found that increasing the content of GNPs gave rise to a dramatic improvement in thermal conductivity from 0.264 W/m·K to 0.7 W/m·K for a 5 wt.% concentration. The outstanding performance of GNPs was due to the planar structure and reduced interfacial thermal resistance, which was also mentioned by Yu et al. (2013). It was shown that the 2-D planar structure of GNPs outperformed the 3-D tubular entangled tubular structure of MWCNTs (Wu et al., 2016).

Metallic nanoparticles were shown to be less effective in improving thermal conductivity. Wang et al. (2009) showed that higher enhancement was achieved at various loadings of Al₂O₃ nanoparticles reaching up to 25% in liquid phase. However, the increase in temperature lowered the thermal conductivity both in liquid and solid phases. Ho and Gao (2009) reported a linear increase in thermal conductivity only up to 9% with increasing Al₂O₃ nanoparticle loadings (5 and 10 wt.%). Increased temperature, particularly at 60°C, led to a higher enhancement in thermal conductivity. This phenomenon was associated by the authors with increased Brownian motion due to decreased viscosity. Jesumathy et al. (2012) showed a gradual increase in thermal conductivity as high as 13% for a 10% wt. CuO-wax nanocomposite at 65°C. The very common trend of a sharp increase in thermal conductivity was detected at the phase change transition from solid to liquid.

Dispersing nanoparticles into PCMs not only enhances thermal conductivity but also leads to a significant increase in the viscosity of the NEPCMs (Yu et al., 2013; Ho & Gao, 2009; Fan et al., 2014). Increased viscosity has a detrimental effect on melting rate due to the

reduction of natural convection, which is a main heat transfer mechanism (Fan et al., 2014). Lokesh et. al (2015) reported that the high loading (0.9 wt.%) of MWCNTs in wax resulted in a significant reduction in solidification time, but longer melting times due to increased viscosity. Therefore, the optimum loading of nanoparticles maximizing the heat conduction enhancement while not compromising the natural convection effect plays a crucial role in NEPCM studies.

Other crucial parameters that caused controversy among researchers are the changes in latent heat capacity and phase change temperature when nanoparticles are added to PCMs. Shaikh et al. (2008) indicated that doping SWCNTs into shell wax at 1 vol.% increased the latent heat capacity up to 13%. Wang et al. (2009) showed a decreased melting temperature and improved latent heat capacity with increasing loadings of MWCNTs in wax. Tang et al. (2014) found that the latent heat of fusion seemed to be increased by more than 10% for 1 and 5 wt.% added f-MWCNTs, whereas 10 wt.% added f-MWCNTs decreased the latent heat capacity, indicating too much f-MWCNTs deteriorates the crystallization growth. Some researchers, on the other hand, reported no change in latent heat capacity with the presence of CNTs (Cui et al., 2011) and xGNP (Kim and Drzal, 2009). However, the majority of studies showed that the addition of nanoparticles gives rise to a significant reduction in latent heat capacity with increasing nanoparticle content (Ho & Gao, 2009; Jesumathy et al., 2012; Teng & Yu, 2012; Fan et al., 2013; Warzoha & Fleischer, 2014; Wu et al., 2016; Nourani et al., 2016(January)). Therefore, this setback affects the storage capacity of thermal storage units that use NEPCMs. Yet, there is another beneficial feature of nanoparticles apart from enhancing thermal conductivity. Supercooling is known to be

one of the unfavorable properties of PCMs where the crystallization of PCMs during solidification occurs at a temperature below its normal freezing point (Al-Shannaq et al., 2015). Thus, recovering the stored energy at the desired temperature becomes difficult, limiting the applications of PCMs. Nanoparticles were found to be very effective in reducing supercooling phenomena by acting as nucleating agents, helping crystallization (Zhang et al., 2011; Kumaresan et al., 2012; Teng & Yu, 2012; Tang et al., 2014; Wu et al., 2016).

2.2.2 Stability of NEPCMs

Another crucial aspect of NEPCMs study is stability. Stability for NEPCMs refers to the uniform dispersion of nanoparticles within the base PCMs without any agglomeration or clusters. This is vitally important for the future of thermal energy storage units with NEPCMs. The marketability of these systems greatly depends on the long-term reliability and consistent high performance of NEPCMs.

There are several methods to evaluate the dispersion quality of nanoparticles in nanofluids and NEPCMs. These methods are mostly based on optical spectroscopy measurement. The scattered light or laser, after being reflected on the sample, is analysed to determine the size distribution, chemical structures, and molecular bonds of nanomaterials within the base fluid (Ghadimi et al., 2011).

Dynamic light scattering (DLS) is widely used to determine the size distribution of small particles in suspension or polymers in a solution. The Rayleigh scattering principle, where a laser is shot through a polarizer into a sample, is applied to collect light scattering data for evaluation. The intensity of the scattering fluctuates as the molecules are moving

constantly due to Brownian motion. Nanoparticle aggregation is tracked over time depending on the sedimentation rate. Sample preparation is paramount for good results. Filtration is vitally important to remove dust and artifacts from the solution. In addition, the temperature needs to be stable during a measurement. Otherwise, convection currents in the sample cause non-random movements which prevent accurate size interpretation (Shaw, 2014).

Ultra-Violet Absorption Spectroscopy (UV-Vis) is a method similar to DLS that analyses the absorbance or emission of electromagnetic radiation by a particle. The collected data on emission reveal the details of the molecular structure. Depending on the transparency and particle distribution, some of the light passes through the sample. The intensity of the reflected light is measured. This is particularly useful for metallic nanoparticles (gold and silver) (Filipponi et al., 2013). The sample's transparency is important to obtaining good data. Because of that, dark samples such as the ones containing CNTs (particularly higher concentrations) are not suitable for this method (Ghadimi et al., 2011).

Another method that aids in examining the stability of nanoparticles is Zeta Potential measurement. Nanoparticles are electrically charged within the base fluid, which gives rise to attraction or repulsion between particles depending on the charge levels (Angayarkanni et al., 2015(September)). If the zeta potential level is above a certain level ($\pm 30\text{mV}$), there will be a push-back force that keeps particles from aggregating. Lower zeta potential values, either positive or negative, refer to unstable conditions due to a lack of repulsive forces. Therefore, the higher the zeta potential value, the more stable the solution (Das et

al., 2007). This method can only be used for polar-based fluids, not for non-polar materials such as the paraffin wax used in this study.

Sedimentation observation through visualization is a very simple and common method, particularly for NEPCMs (Ghadimi et al., 2011; Das et al., 2007). Nanoparticle stability is examined via capturing pictures of samples repeatedly over time or thermal cycles. Sedimentation levels of samples are then compared from the images.

Most of the studies considered the stability of NEPCMs through the sedimentation observation method. Kumerasan et al. (2012) did a visual inspection of MWCNTs-dispersed paraffin wax to monitor stability. They claimed visually stable samples for various concentrations after three months. Tang et al. (2014) found that the stability of f-MWCNTs through acid treatment with octadecylamine in toluene was much better without any visible settlement than that of crude MWCNTs. DSC analysis also showed that cyclic stability was maintained after 100 thermal cycles without any significant change in latent heat capacity, phase change temperature and supercooling. Another study on the dispersion of MWCNTs in paraffin wax was carried out by Wang et al. (2009). Ball-milling treated MWCNTs were found to be homogeneously dispersed without any lamination through Scanning Electron Microscope (SEM) images after being kept in an oven at 70°C for 96 h. Angayarkanni and Philip (2015, June) observed the change in thermal conductivity of GNPs and MWCNTs dispersed in wax over five thermal cycles. They found that thermal conductivity enhancement fluctuated and then gradually decreased for solid phase at 10°C as nanocomposites underwent thermal cycles. Yu et al. (2013) did Transmission Electron Microscope (TEM) imaging to study the dispersion quality of various nanoparticles in

paraffin wax. TEM imaging revealed that highly agglomerated dispersion was the case for GNPs and CNFs and long MWCNTs due to their large particle size. Relatively better dispersion was attained for carboxyl functionalized-short MWCNTs and short MWCNTs. The stability of prepared samples was observed for the highest concentration of nanoparticles (4 wt.%) assuming the tendency of agglomeration and sedimentation is higher for most concentrated samples. It was seen that samples were visually stable after 1.5 h, providing sufficient time to make thermal conductivity and viscosity measurements. Nevertheless, after a day, the GNPs and the other nanoparticles were found to be settling and forming clusters. Zhang et al. (2011) investigated the suspension time of untreated and surface-treated MWCNTs with various surfactants in n-hexadecane. Surface-treated MWCNTs with 1-decanol provided the longest suspension time (290 min) compared to other combinations. The cyclic stability of CNTs added 1-dodecanol was examined visually by Zeng et. al (2013). Specimens were found to be settlement-free after two melting/solidification cycles. With the third cycles, sedimentation took place. However, specimens were observed to maintain desired stability in liquid phase for several days.

A shape stabilization study of GNP-paraffin wax nanocomposites was done by Shi et al. (2013). They found that GNPs played an important role in increasing the dropping point temperature of paraffin wax. The 2 wt.% GNP-paraffin wax sample kept its form without any leakage up to 185.2°C, indicating the possibility of using GNP-paraffin wax nanocomposite as an energy storage material without a container. Fan et al. (2014) pointed out that GNPs' dispersion in 1-tetradecanol substantially improved its stability up to 5 melting/solidification thermal cycles due to the presence of a commercial dispersant.

However, further thermal cycles caused significant precipitation. Fang et al. (2013) claimed good dispersion of GNP-eicosane samples. However, long-term stability was not concerned as measurements were done in solid phase. Mehrali et al. (2013) impregnated paraffin wax into graphene oxide (GO) sheets to create stabilized nanocomposites for thermal energy storage systems. DSC measurements revealed that the nanocomposites maintained their properties; specifically, latent heat and phase change temperature with only slight deviations up to 2500 thermal cycles.

Weinstein et. al. (2008) had to use sonication between tests to avoid the settlement of graphite in wax. Zheng et al. (2010) examined the suspension quality of graphite particles in hexadecane at a low concentration (0.05 wt.%). Overall, the suspension of graphite flakes was maintained, providing the percolation network both in liquid and solid phase. Wu et. al. (2010) dispersed Cu, Al, and C/Cu nanoparticles into paraffin wax with different surfactants to see the effects on thermal properties and stability. Samples with Hitenol BC-10 surfactant were found to be most stable after 12 h by visual inspection. Nanocomposites were observed to be stable in terms of phase change temperature and latent heat capacity after 100 thermal cycles. Jesumathy et al. (2012) claimed no settling for CuO-dispersed paraffin wax after applying intense sonication for 6 h. Fan and Khodadadi (2011, March) detected significant sedimentation visually for 2 vol.% CuO-cyclohexane after several freezing/melting cycles despite the usage of Sodium Oleate to promote stability. A similar study by Nabil and Khodadadi (2013) applied the same procedure in preparing the CuO doped eicosane samples. They claimed stable samples even at a 10 wt.% concentration. Nourani et. al. (2016, March) conducted a stability study of Al₂O₃ dispersed paraffin wax

using image analysis. They found that the sedimentation rate increased proportionally as the samples underwent up to 25 melting/solidification cycles. They also performed thermal cycles using DSC between 25 and 70°C. No significant change in melting temperature and latent heat capacity was observed over 120 thermal cycles.

Table 2.1: Summary of PCM type, nanoparticle type, size and fraction

Authors (year)	Base PCM and Properties	Nanoparticle Enhancers		
		Material	Dimensions	Fraction of enhancers
Elgafy and Lafdi (2005)	Paraffin wax T_m : 67°C	CNF	Diameter: 100 nm Length: 20 μ m	1, 2, 3, and, 4 wt.%
Shaikh et al. (2008)	Shell wax 100 T_m : N/A	SWCNT MWCNT CNF	Diameter: 1 nm Diameter: 10 nm Diameter: 100 nm	0.1, 0.4, 0.7, and 1 vol.%
Weinstein et al. (2008)	Paraffin wax T_m : 56°C	Graphite	Diameter: 4-10 nm Length: 1 μ m	0.25, 0.5, 1, and 5%
Kim and Drzal (2009)	n-docosane T_m : 53-57°C	xGNP	Diameter: 15 μ m Thickness:< 10nm	1, 2, 3, 5, and 7 wt.%
Ho and Gao (2009)	n-octadecane T_m : 25-28°C	Al ₂ O ₃	Diameter: 159.6-196 nm	5 and 10 wt.%
Wang et al. (2009)	Paraffin wax T_m : 52-54°C	MWCNT	Diameter: 30 nm Length: 50 μ m	0.2, 0.5, 1, and 2 wt.%
Wang et al. (2010)	Paraffin wax T_m : 52-54°C	γ -Al ₂ O ₃	Diameter: 20 nm	1, 2, and 5 wt.%
Wu et al. (2010)	Paraffin wax T_m : 58-60°C	Cu, Al, C/Cu powders	Average size: 25 nm	0.5, 1, and 2 wt.%
Zheng et al. (2010)	Hexadecane T_m : 18°C	Graphite	Planar distance: 0.335nm	0.2, 0.4, 0.6, 0.8, 1 vol.%

Fan and Khodadadi (2011)	Cyclohexane T _m : 6°C	CuO	Diameter: 5-15 nm	0.5, 1, and 2 vol.%
Cui et al. (2011)	Paraffin and soy wax T _m : 52-54°C	CNF CNT	Diameter: 200nm Diameter: 30 nm Length: 50 µm Surface area: 60 m ² /g	1, 2, 3, 5, and 10 wt.%
Zhang et al. (2012)	Hexadecane T _m : 18°C	MWCNT	Diameter: 10-20 nm Length: 0.5-2 µm	0.1, 0.5, 1, 2, 10 wt.%
Jesumathy et al. (2012)	Paraffin wax T _m : 58°C	CuO	Mean size: 40 nm	2, 5, and 10 wt.%
Teng and Yu (2012)	Paraffin wax T _m : 55-65°C	Al ₂ O ₃ , SiO ₂ , TiO ₂ , ZnO	Size: 20-30 nm, 100-400 nm	1, 2, and 3 wt.%
Teng et al. (2012)	Paraffin wax T _m : 54-60°C	MWCNT Graphite	Size: 20-30 nm Size: 3.2 µm	1, 2, and 3 wt.%
Kumaresan et al. (2012)	Paraffin wax T _m : 19-22°C	MWCNT	Diameter: 30-50 nm Length: 10-20 µm Surface area: 60 m ² /g	0.15, 0.3, 0.45, and 0.6 vol.%
Shi et al. (2013)	Paraffin wax T _m : 61.6°C	xGnP	Size: 700µm (before exfoliation)	1, 2, 5 and 10 wt.%
Yu et al. (2013)	Paraffin wax T _m : 58-60°C	S-MWCNT C-SMWCNT L-MWCNT CNF GNP	Diameter: 8-15 nm Length: 0.5-2 µm Diameter: <10 nm, Length: 5-15 µm Diameter: 150-200 nm Length: 10-30 µm Diameter: 5-10 µm Thickness: 4-20 nm	1, 2, 3, and 4 wt.%
Mehrali et al. (2013)	Paraffin wax T _m : 50-60°C	Graphite	Size: 3.2 µm	51.7, 52.2, 52.61, and 55.19 wt.%

Nabil and Khodadadi (2013)	Eicosane T_m : 37°C	CuO	Diameter: 5-15 nm	1, 2, 3.5, 5, 6.5, 8 and 10 wt. %
Fan et al. (2013)	Paraffin wax T_m : 59°C	S-MWCNT C-SMWCNT L-MWCNT CNF GNP	Diameter: 8-15 nm Length: 0.5-2 μ m Diameter: 30-50 nm, Length: 5-15 μ m Diameter: 150-200 nm Length: 10-30 μ m Diameter: 5-10 μ m Thickness: 4-20 nm	1, 2, 3, 4 and 5 wt. %
Fang et al. (2013)	Eicosane T_m : 37°C	GNP	Diameter: 5-10 μ m Thickness: 4-20 nm	1, 2, 5, and 10 wt. %
Zeng et al. (2013)	1-dodecanol (C ₁₂ H ₂₆ O) T_m : 37°C	MWCNT	Diameter: 8-15 nm Length: 0.5-2 μ m	1 and 2 wt. %
Warzoha and Fleischer (2014)	Paraffin wax T_m : 56.15°C	Graphene MWCNT Al TiO ₂	Thickness: 4-20 nm Length: 25 μ m Diameter: 50-80 nm Length: 10-20 μ m Diameter: 40 nm Diameter: 30 nm	20 vol. %
Tang et al. (2014)	Paraffin wax T_m : 52-54°C	MWCNT	Diameter: 10-20 nm	1, 5, and 10 wt. %
Fan et al. (2014)	1-tetradecanol (C ₁₄ H ₃₀ O)	GNP	Diameter: 5-10 μ m Thickness: 4-20 nm	0.5, 1, and 3 wt. %
Yang et al. (2014)	Paraffin wax T_m : 56-58°C	Si ₃ N ₄	N/A	1, 2, 3, 4, 5 and 10 wt. %
Angayarkanni and Philip (2015)	Hexadecane T_m : 18°C	MWCNT GNP CuNW	Diameter: < 8 nm Length: 10-30 μ m Size: 2 μ m Thickness: 1-4 nm Diameter: 50 nm	0.005, 0.0075, 0.01, 0.05, 0.1, 0.2, and 0.5 wt. %

			Length: 10-50 μm	
Lokesh et al. (2015)	Paraffin wax T_m : 50-59°C	MWCNT	Diameter: 30- 50 nm Length: 10-20 nm Surface area: 60 m^2/g	0.3, 0.6, and 0.9 wt. %
Nourani et al. (2016, January)	Paraffin wax T_m : 54-58°C	Al_2O_3	Size: 10-20 nm	2.5, 5, 7.5, and 10 wt. %
Nourani et al. (2016, March)	Paraffin wax T_m : 54-58°C	Al_2O_3	Size: 10-20 nm	2.5, 5, 7.5, and 10 wt. %
Wu et al. (2016)	Paraffin wax T_m : 58-60°C	GNP-B GNP-C MWCNT G-MWCNT	Diameter: 100-200 nm Thickness: 0.335 nm Diameter: 5-10 μm Thickness: 4-20 nm Diameter: 8-20 nm Length: >50 nm	0.2, 0.5, 1, 2 and 3 wt. %

Table 2.2: Summary of preparation, characterization, heat transfer study and stability of NEPCM

Authors (year)	Dispersion Method	Characterization		Heat Transfer Study	Stability
		Thermal Conductivity measurement method	Other measurements and instruments		
Elgafy and Lafdi (2005)	Shear mixing	Laser flash technique	DSC	Monitoring solidification performance using thermocouples.	N/A
Shaikh et al. (2008)	Shear mixing, sonication for 4 h	N/A	DSC	N/A	N/A
Weinstein et al. (2008)				Monitoring melting	Significant settling

	Sonication for 4 h	Fourier's Law	DSC	performance using thermocouples in a cube.	observed visually after the third melting/freezing cycle.
Kim and Drzal (2009)	Stirring, Particle treatment: Exfoliation in obtaining xGnPs	Guarded heat flow meter method (UNITHERM Model 22)	SEM, DSC, TGA	N/A	N/A
Ho and Gao (2009)	Sonication for at least 3h, surfactant coating (1:3 mass ratio to particle mass)	THW (KD2 Thermal Analyzer)	DSC, viscometer	N/A	N/A
Wang et al. (2009)	Ball milling for 9 h, Intensive sonication	TSHW	DSC, SEM	N/A	No lamination claimed through SEM pictures after being kept in an oven at 70°C for 96 h.
Wang et al. (2010)	Intensive sonication, Surfactant: Oleylamine (amount unknown)	TSHW	DSC, TEM, SEM, XRD, FTIR	N/A	N/A
Wu et al. (2010)	Sonication for 2 h, Surfactants: CTAB, GA, Span-80, SDBS, Hitenol BC-10	N/A	DSC, FTIR	Monitoring the heating/cooling performance.	Thermal stability tests through 100 cycles of melting/freezing. Most visually stable samples are obtained with Hitenol BC-10.
Zheng et al. (2010)					Stability observation

	Particle treatment: chemical intercalation, thermal expansion Sonication for 15 min	THW	Electrical conductivity	N/A	through thermal conductivity measurement after several freezing/melting cycles. Insignificant change in measurements over cycles.
Fan and Khodadadi (2011)	Mixing for 30 min Surfactant: Sodium oleate (amount unknown)	N/A	N/A	Monitoring freezing using thermocouples and comparing with a 1-D Stefan model.	Significant sedimentation after several freezing/thawing for 2 vol.% NEPCM.
Cui et al. (2011)	High-speed stirring for 30 min followed by sonication for 1 h	THW (KD2 Thermal Analyzer)	DSC, SEM	Monitoring heating/cooling performance using thermocouples.	N/A
Zhang et al. (2012)	Particle treatment: surface modification through acid treatment Sonication for 5 min Surfactants: SDS, CTAB, PVA, PEG, TEMED, TEA, AcCOOH, SA, 1-decanol, Tween-80, Triton X-100	N/A	DSC, FTIR, DLS	N/A	Stability observation through suspension time. Surface-treated MWCNT-1-decanol combination provided the longest suspension time.
Jesumathy et al. (2012)	Sonication for 6 h	THW (KD2 Thermal Analyzer)	DSC, viscometer	Monitoring charging/discharging performance	Stable samples with no visual settling.

				using thermocouples.	
Teng and Yu (2012)	Stirring, High-speed homogenizing for 40 min followed by sonication for 1 h	N/A	DSC, FTIR	Monitoring solidification performance using a thermocouple.	N/A
Teng et al. (2012)	Stirring, High-speed homogenizing for 40 min followed by sonication for 1 h	N/A	DSC	Monitoring charging/discharging performance using thermocouples	N/A
Kumaresan et al. (2012)	Pre-dry sonication for 90 min with nanoparticles followed by 30 min sonication	THW (KD2 Thermal Analyzer)	DSC, TEM, SEM, viscometer	Monitoring melting/freezing performance using thermocouples	Visually stable samples were claimed after 3 months.
Shi et al. (2013)	Particle treatment: Acid intercalation, exfoliation, sonication for 30 min	TPS (Hot Disk Analyzer, TPS 1500)	DSC, XRD, SEM	N/A	Shape-stabilization test (dropping temperature point)
Yu et al. (2013)	Stirring for 15 min followed by sonication for 50 min	THW (KD2 Thermal Analyzer)	SEM, TEM, AFM, viscometer	N/A	Degrading stability observation with time for higher concentrations due to agglomeration.
Mehrali et al. (2013)	Particle treatment: Producing Graphene oxide sheet using	THW (KD2 Thermal Analyzer)	DSC, SEM, FTIR,	N/A	Thermally stable after melting/freezing tests up to 2500 cycles.

	Brodie's method, Vacuum impregnation for 2 h under 100 kPa				
Nabil and Khodadadi (2013)	Mixing for 30 min Surfactant: Sodium oleate (amount unknown)	TPS (Hot Disk Analyzer, TPS 500)	N/A	N/A	No significant precipitation was claimed even for most concentrated sample (10 wt.%).
Fan et al. (2013)	Stirring for 15 min followed by sonication for 50 min	THW (KD2 Thermal Analyzer)	DSC, SEM, AFM	N/A	N/A
Fang et al. (2013)	Stirring for 15 min followed by sonication for 30 min	TPS (Hot Disk Analyzer, TPS 2500)	DSC, SEM, AFM	N/A	Good visual dispersion was claimed after preparation for solid phase.
Zeng et al. (2013)	Stirring for 30 min followed by sonication for 30 min, Commercial dispersant (1:1 mass ratio, unknown)	TPS (Hot Disk Analyzer, TPS 2500)	DSC, viscometer	Monitoring melting performance in a cylindrical cavity using thermocouples.	Visually stable samples after 2 thermal cycles. Long-term stability claimed in liquid phase for several days.
Warzoha and Fleischer (2014)	Sonication for 20 min	TPS (Hot Disk Analyzer, TPS 2500)	DSC	Monitoring charging/discharging performance in thermal containment unit using thermocouples	N/A
Tang et al. (2014)	Particle treatment: carboxylation			Monitoring charging/discharging performance	Thermal stability tests of

	n and functionalization using n-octadecylamine, sonication for 1 h	TPS (Hot Disk Analyzer, TPS 2500)	DSC, SEM, FTIR, TEM, XRD	using thermocouples	melting/freezing up to 100 cycles, Better visual stability with functionalized MWCNT compared to crude MWCNT.
Fan et al. (2014)	Stirring for 15 min followed by sonication for 30 min, Commercial dispersant (1:1 mass ratio, unknown)	TPS	DSC, viscometer	Monitoring melting performance in a cylindrical cavity using thermocouples, Simplified analysis of heat transfer through non-dimensionless numbers (Fourier, Stephan, Rayleigh and Nusselt numbers).	Significant precipitation was observed after 5 melting/freezing thermal cycles.
Yang et al. (2014)	Stirring with ultrasonic wave for 30 min	THB (THB-Instrument, Linseis)	DSC, 3D microscope	N/A	N/A
Angayarkanni and Philip (2015)	Sonication for 30 min, Acid treatment for GNP Surfactant: 2 wt % oleylamine	TPS (Hot Disk Analyzer, TPS 2500)	TEM	N/A	Stability evaluation based on thermal conductivity change after 5 thermal cycles.
Lokesh et al. (2015)	Stirring for 30 min followed by sonication for 90 min	THW (KD2 Thermal Analyzer)	TEM	Monitoring melting/freezing performance using thermocouples.	N/A
Nourani et al. (2016, January)	Stirring for 1 h, Sonication for 2 h	THW	DSC	Monitoring heating rate using thermocouples.	Thermal stability tests of melting/freezing

	Surfactant: Sodium stearoly lactylate (1:3.5 mass ratio)				ng up to 120 cycles.
Nourani et al. (2016, March)	Stirring for 1 h, Sonication for 2 h Surfactant: Sodium stearoly lactylate (1:3.5 mass ratio)	N/A	FTIR, UV-Vis	N/A	Image Analysis after 25 melting/solidif ication cycles.
Wu et al. (2016)	Stirring for 15 min followed by sonication for 1 h	TPS	DSC, SEM	Monitoring melting/freezing performance using thermocouples.	N/A

2.3 Literature Summary

The first part of the literature review focused on the latent heat thermal energy storage with PCM, particularly involving a helical coil heat exchanger configuration. Some of the major outcomes from the literature review can be summarized as follows:

- HTF inlet temperature has a greater effect on the charging/discharging times than the HTF volume flow rate.
- Although the increase in the HTF volume flow rate decreases the charging time, it does not have any influence on the discharging time.
- Natural convection dominates the charging process with an increasing melted portion, while conduction is the main mode of heat transfer during discharging.

- The effect of flow direction for a vertical helical coil configuration has not been broadly reported or investigated.

The second part of the literature review is dedicated to NEPCM studies. Significant findings are presented as follows:

- There seems to be no standard for the preparation of NEPCMs. Although the dispersion of nanoparticles is mainly achieved through mechanical (stirring and sonication) and chemical (surfactants) methods, the duration and intensity of stirring or sonication as well as the selection (type) and the amount of surfactant used vary greatly. Determining these crucial parameters is generally not reasoned.
- Carbon-based nanoparticles, particularly GNPs, perform better than metallic nanoparticles in enhancing thermal conductivity.
- Thermal conductivity enhancement results were usually obtained when the samples were at the most stable state. Therefore, measurements should be repeated over melting/solidification cycles. But most previous studies did not conduct cyclic measurements.
- Some studies evaluated the stability of NEPCMs based on DSC results. DSC analysis is done for only a very small amount of NEPCM which lacks information on how particle agglomeration occurs in bulk.
- Maintaining uniform dispersion of nanoparticles in PCMs without any settlement is a great challenge that needs to be studied further.

Chapter 3 Experimental Research on LHTESS with Paraffin

Wax as a PCM

In this chapter, the performance of a helical coil heat exchanger TES unit was analyzed. Charging and discharging tests were carried out under different operational conditions. Melting and solidification characteristics of the PCM in the storage were presented. The fabrication and design procedures were briefly mentioned. The experimental results and discussions that shaped the following research efforts in the next chapters were reported.

3.1 PCM Heat Exchanger and Experimental Setup

3.1.1 Theoretical design of the thermal energy storage unit

Actual melting and solidification processes involve both latent heat and sensible heat due to the temperature change of the PCM. The amount of heat stored can be theoretically calculated with Equation (1).

$$Q_{stored} = m_{pcm} [C_{p,pcm,s}(T_m - T_i) + H_{pcm} + C_{p,pcm,l}(T_f - T_m)] \quad (1)$$

where m_{pcm} is the mass of the paraffin wax, H_{pcm} is the latent heat capacity of the paraffin wax, T_i is the initial temperature of the wax, T_m is the melting temperature of the wax, T_f is the final temperature of the wax at the end of charging, and $C_{p,pcm,s}$ and $C_{p,pcm,l}$ are the specific heat of the wax in both solid and liquid phases, respectively. The latent and sensible energy calculations for wax assumed that the temperature of the wax is increased from 18°C to 70°C. The values of these parameters are summarized in Table 3.1.

The total energy supplied and recovered from the storage unit during charging and discharging was found by calculating the 20-second period of energy inputs/outputs over the charging and discharging time using the formulae as follows;

$$Q_{total} = \sum \Delta t \times \dot{m}_{HTF} \times C_{p,HTF} \times \Delta T \quad (2)$$

where \dot{m}_{HTF} and $C_{p,HTF}$ stand for the mass flow rate and specific heat of heat transfer fluid.

ΔT is the temperature difference between inlet and outlet thermocouples.

Table 3.1: Properties of PCM and HTF (Ukrainczyk et al., 2010)

m_{pcm}	3.54 kg
k_{pcm}	0.34W/m K(solid), 0.28W/m K(liquid)
$C_{p,pcm,s}$	2.6 J/g·K
$C_{p,pcm,l}$	2.981 J/g·K
H_{pcm}	160 kJ/kg
T_i	18°C
T_m	51°C
T_f	70°C
\dot{m}_{HTF}	0.07-0.00875 kg/s
$C_{p,HTF}$	3.56 J/g·K

3.1.2 Design and fabrication of the helical coil heat exchanger thermal energy storage unit

An overall shell-and-tube heat exchanger layout was selected for the prototype design. Different concepts for the tube configuration, HTF pattern, and insulation were considered and evaluated (Duan et al., 2016). The final selection of design parameters is summarized here. Paraffin wax was selected as the phase change material. Paraffin wax has an excellent latent heat of fusion, with a desirable operating temperature range (~50 °C) for warm water applications. Single phase of ethylene glycol (EG)-water was selected as the heat transfer fluid (HTF) due to its low cost, availability, and higher safety in handling. For the tank

shell, polycarbonate was selected for this experimental prototype. Polycarbonate is durable, widely available, and easy to use with great heat/corrosion resistance. In addition, this material inherently acts as pseudo-insulator as it has a low thermal conductivity. With good transparency, this material also allows monitoring of the PCM melting and solidification process during lab testing. A helical tube design was chosen for final fabrication. Preliminary CFD simulation and lab testing proved that the spiral tube has better heat transfer performance than straight tubing (Duan et al., 2016). Copper was chosen for the HTF tube due to its exceptionally high thermal conductivity, low cost, and availability.

The final design of the storage has the following dimensions: 30.54 cm (1 ft) in length and 16.64 cm (6.55 in) in outer diameter. The top and bottom ends of the container were attached to square grooved acrylic plates with a thickness of 0.9525 cm (3/8 in) and length of 19.05 cm (7.5 in) (Figure 3.1-(a)). Four holes were drilled near each corner of the plates for stainless steel rods later to be inserted through to hold the heat exchanger together by fastening the nuts. Three additional holes were drilled to accommodate thermocouples, an alignment rod to keep the helical coil inline, and an opening for PCM filling and draining purposes. The shell was covered with an insulation blanket made of cryogel, an advanced insulation material, (Scotia Insulations Co.) including top and the bottom plates to prevent heat loss. Helical coil tubing was made from a 315-cm (124 in) long copper pipe with an inner and outer diameter of 0.635 cm (1/4 in) and 0.952 cm (3/8 in), respectively. The coil diameter was chosen as 10.16 cm (4 in) with a pitch of 2.8575 cm (1.125 in) yielding 8.7 turns and 7.62-cm (3 in) long straight tubing extending from the center of the helical coil

at each end (Figure 3.1-(b)). The fully prepared PCM thermal energy storage unit with insulation is shown in Figure 3.1-(c).

After placing the helical coil inside the storage tank, the heat exchanger prototype was sealed using a silicon caulking. Silicon seals were made between the end-caps and the Lexan shell and between the plastic tubing and end-cap penetrations. Paraffin wax was poured into the storage in liquid phase through the filling hole. After pouring the molten wax into the shell, the whole setup was cooled at room temperature to let the PCM completely solidify for lab testing.

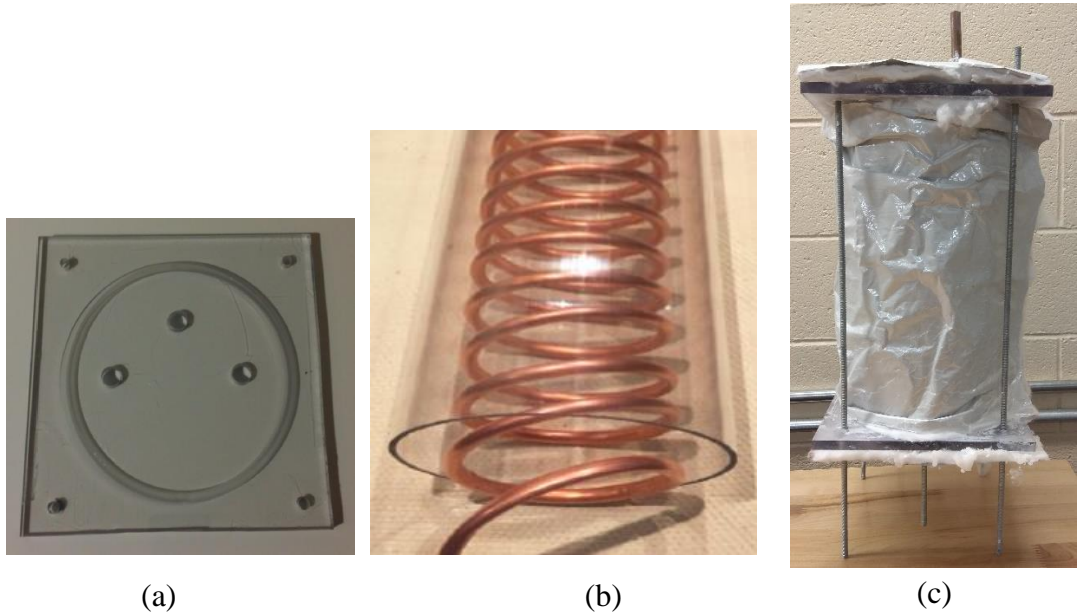


Figure 3.1: Fabrication of the heat exchanger and the storage tank.

3.1.3 Experimental setup

A schematic of the experimental setup is shown in Figure 3.2-(a). The main components include the cylindrical PCM heat exchanger with helical tubing, a thermal bath circulator, and a computer (PC) with a data acquisition system (DAQ). The thermal bath circulator

provides EG-water as HTF at desired temperatures for both charging and discharging. The outlet of the thermal bath is connected to a three-way ball valve which allows for adjustment of the flow rate of the HTF. The flow rate of the HTF is monitored using a flow meter connected to the inlet line of the storage unit. The excess amount of HTF is directed back to the thermal bath through a bypass line. The outlet pipe connected to the top of the storage merges with the bypass line going back to the thermal bath. The thermocouples and flow meter were connected to the DAQ system to record measured data on the computer.

Six T-type thermocouples were used for tracking the temperature profile within the storage unit. Three thermocouples were located at three different heights in the center of the container while two thermocouples were used for monitoring the inlet and outlet HTF temperature (Figure 3.2-(b)). The bottom thermocouple was positioned 2.22 cm (0.875 in) above the bottom plate in the center. The middle thermocouple was attached to the same rod as the bottom center thermocouple at 17.46 cm (6.875 in) height. The top thermocouple was placed just an inch (2.54 cm) above the middle thermocouple due to significant shrinkage upon solidification. The last thermocouple was also inserted at the same height as the bottom center thermocouple but 6.35 cm apart from it to measure the radial temperature difference. The thermocouples were calibrated by comparing the measured values with the pre-manufactured thermocouple's measurements. The uncertainty was found to be ± 1 °C, which is acceptable for this experimental study.

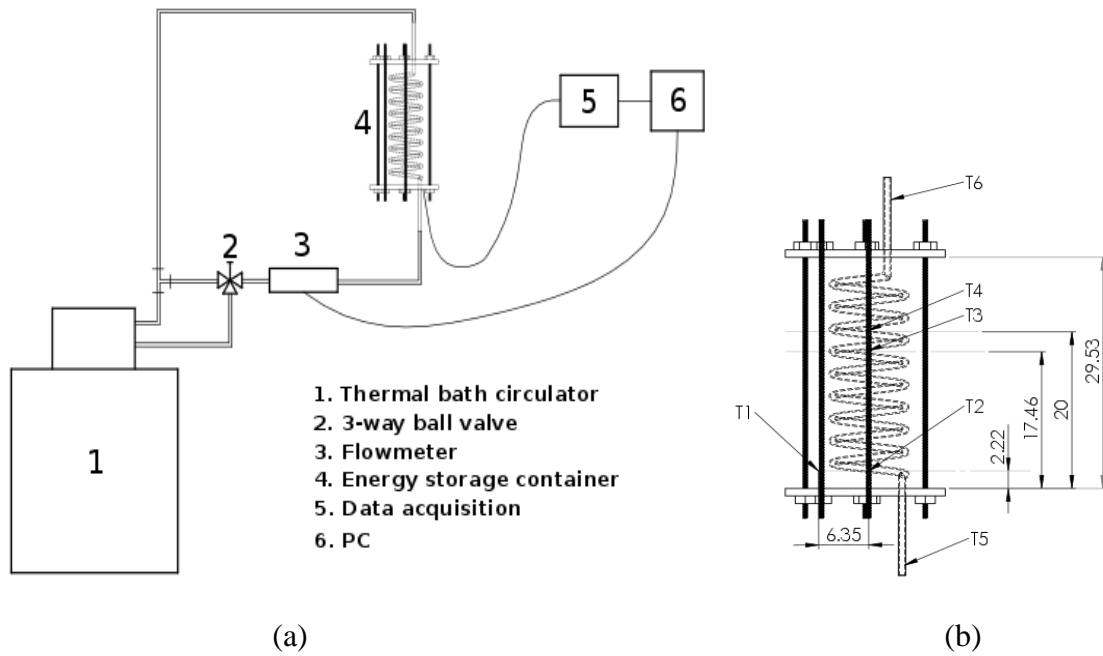


Figure 3.2: (a) Schematic of the experimental setup; (b) Positions of thermocouples; T1: Side bottom, T2: Center bottom, T3: Center middle, T4: Center top, T5: HTF inlet, T6: HTF outlet.

3.2 Experimental Results and Discussions

This section presents the results of the experiments under different operational conditions. Three main parameters, namely, HTF flow rate, HTF inlet temperature and HTF flow direction, were investigated. Many studies have examined these factors for helical coil heat exchanger thermal energy storages (Korti & Tlemsani, 2016; Sundaram et al., 2016; Tayssir et al.; 2016; Zhang et al., 2017; Yang et al., 2017). Although there is agreement on the fact that inlet HTF temperature has a greater effect on the charging time than the HTF flow rate, the effect of the inlet HTF position seems to be the missing point which needs to be further studied. Experiments aimed to determine the effect of each parameter on charging and discharging time. The ranges of these parameters were chosen based on the capability of the thermal bath. The operational conditions of 11 tests were summarized in Table 3.2.

Figure 3.3 also shows the comparison of charging and discharging times for the tests. It should be noted that only a few illustrations to demonstrate the common outcomes of the tests are given in the subsequent sections. However, the discussion section includes all experimental tests and different conditions.

Table 3.2: Outline of the experiments under different operational conditions

Experiment number	Experiment type	Flow rate, LPM	Inlet temperature, °C	Flow direction
Test 1	Charging	4	75	Upward
Test 2	Charging	2	75	Upward
Test 3	Charging	1	75	Upward
Test 4	Charging	0.5	75	Upward
Test 5	Charging	4	70	Upward
Test 6	Charging	4	75	Downward
Test 7	Discharging	2	20	Upward
Test 8	Discharging	1.5	20	Upward
Test 9	Discharging	1	20	Upward
Test 10	Discharging	0.5	20	Upward
Test 11	Discharging	1.5	20	Downward

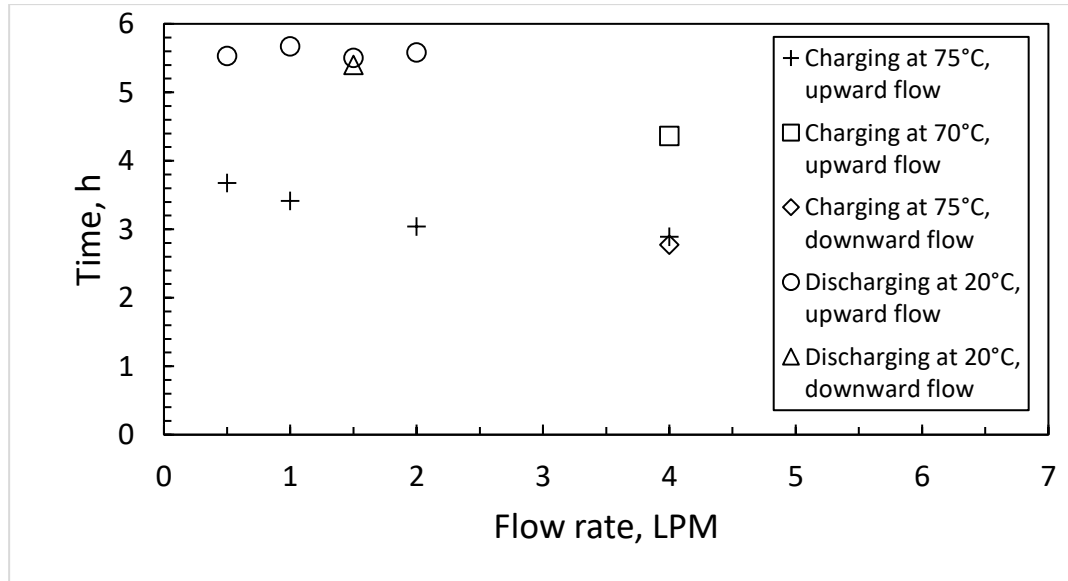


Figure 3.3: Comparison of charging and discharging times at different operational conditions.

3.2.1 Charging

Charging tests were carried out to investigate the melting behavior and how the phase change evolves inside the storage unit. Figure 3.4 shows the temperature profile of paraffin wax at different locations with an HTF flow rate of 4L/min at a 75°C inlet temperature. The melting behavior was observed through capturing images every half an hour to track the liquid/solid interface (Figure 3.5). At the beginning of charging, it was seen that the melting starts from the proximity of the helical coil as a heat source since the side bottom thermocouple reads higher temperatures than other thermocouples in the center (Figure 3.4). As the melted portion grew, the liquid wax was pushed upward by buoyant force initiating natural convection, which is the dominant heat transfer mechanism onwards (Figure 3.5-B). This behavior explains the phenomenon observed in Figure 3.5-C where a big chunk of mountain-shaped wax was located at the center of the cylinder. In the late stage of the charging process, the abrupt increase in temperature on the top and middle thermocouples in the center was caused by increased heat transfer with natural convection. Meanwhile, the temperature at the bottom increased linearly due to conduction heat transfer. The rate of temperature increase at the top and middle thermocouples slowed after the sudden increase as more energy was supplied from the HTF to the phase change process rather than increasing the temperature at these points. It was evident that a steep temperature increase at the top and middle thermocouples was present once the melting front passed these probe locations and moved downwards over time (Figure 3.5-D-E). This could be attributed to the significantly less energy required to increase the temperature of the PCM as opposed to causing phase change from solid to liquid. The conical-shaped big chunk of wax underwent the phase change process and gradually disappeared (Figure 3.5-

D-E-F). Finally, the same sudden temperature increase was seen for the thermocouples at the bottom, with the one in the center being more distinct.

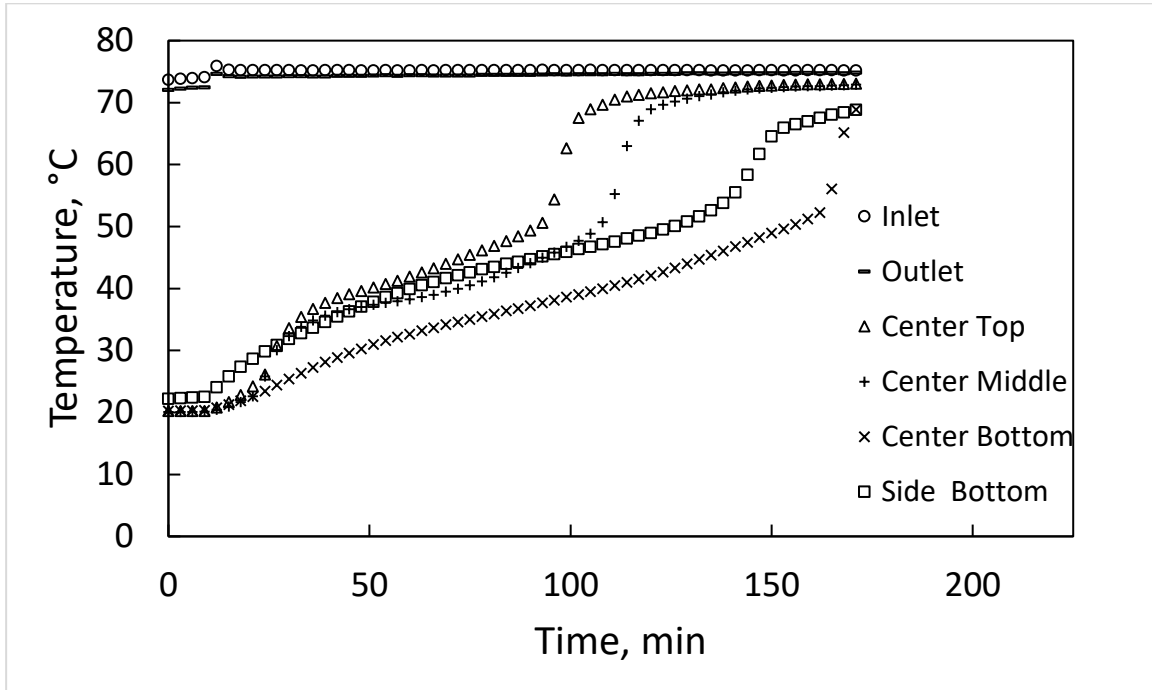


Figure 3.4: Charging with a flow rate of 4 LPM at a 75°C HTF inlet temperature.

3.2.2 Discharging

Figure 3.6 shows the temperature variations in the storage unit during discharging with a HTF flow rate of 1 L/min at a 20°C inlet temperature. A significant drop in temperature for all the thermocouples was noted at the beginning of discharging due to sensible energy loss. This resulted in a significant temperature difference between inlet and outlet HTF. Solidification started from the outer surface of the helical coil and inner wall of the container due to heat loss. The onset of solidification obstructed observation of the solidification behavior of the inner layers of the PCM (Figure 3.7). The solidification rate dropped in response to the growing solidified region acting as insulation.

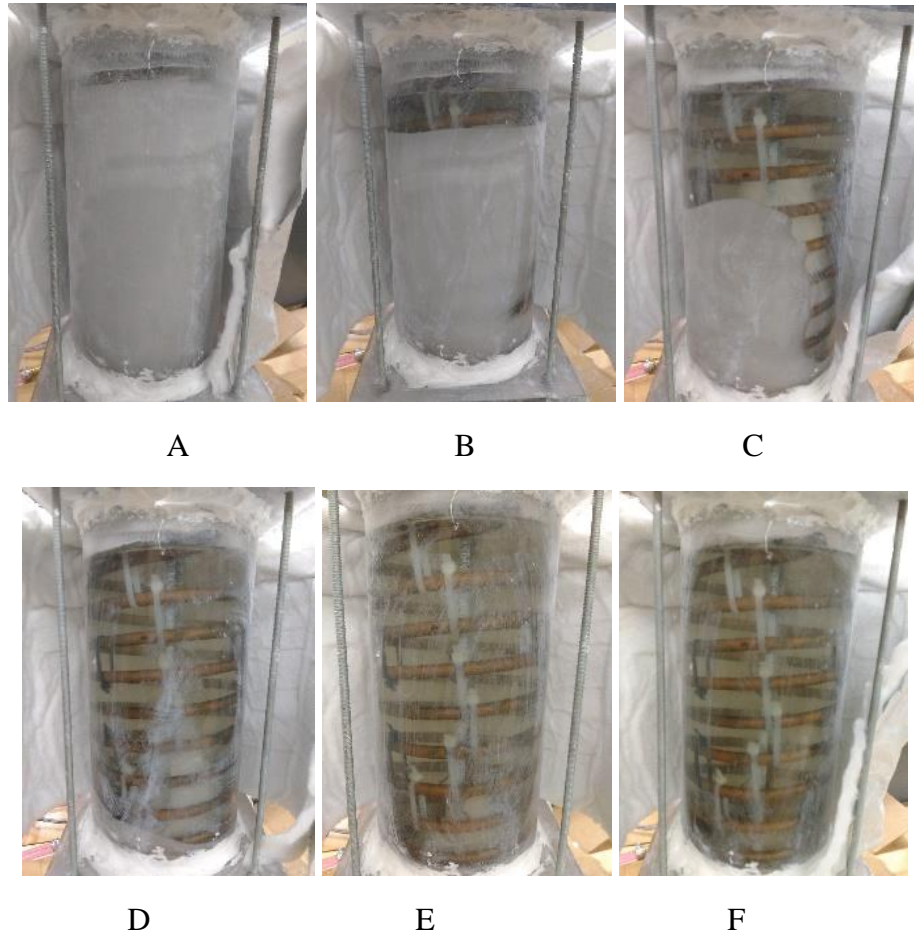


Figure 3.5: Pictures of charging with a flow rate of 4 LPM at 75°C (A: 30 min, B: 60 min, C: 90 min, D: 120 min, E: 145 min, F: 170 min).

As can be seen from Figure 3.6, the liquid-solid transformation took place at around 55°C. The foreign structures within the storage such as metal rods placed in the container provided a heterogeneous nucleation site that requires slight supercooling to initiate the solidification. The side bottom thermocouple readings diverged from the ones in the center and decreased rapidly right after completing the phase change due to its proximity to the helical coil. The heat extracted from the PCM decreased drastically, leading to an insignificant temperature difference between inlet and outlet HTF due to increased thermal resistance in the solid layer. The completion of the phase change was followed by a gradual

cool down to a cold HTF temperature with the center middle thermocouple being the slowest.

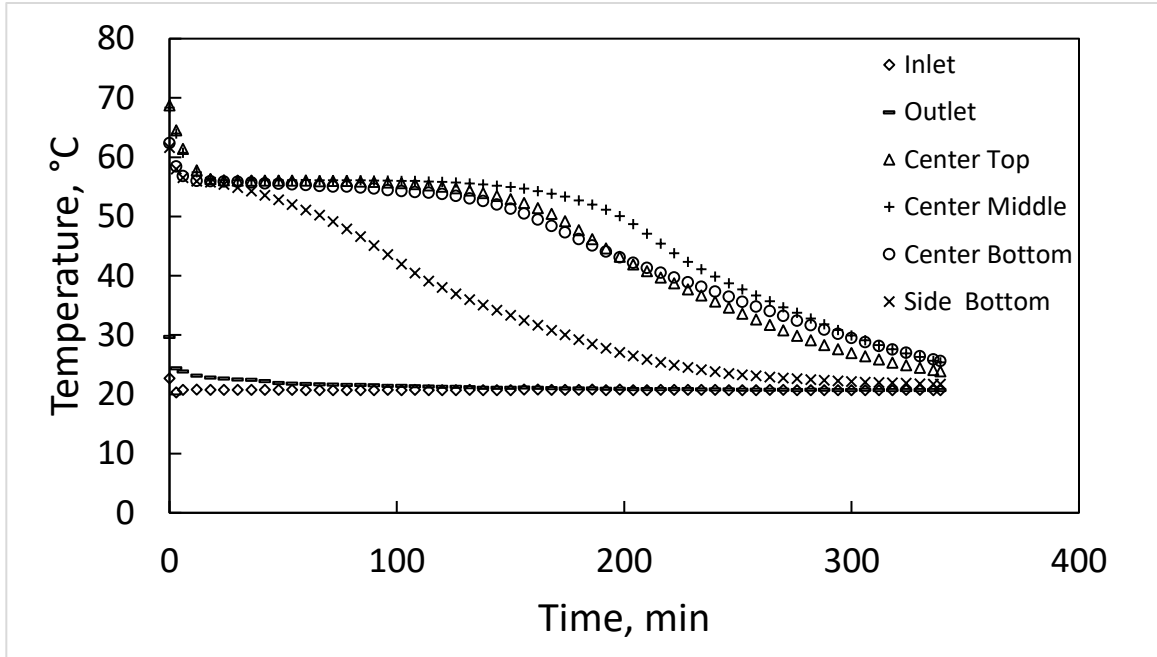


Figure 3.6: Discharging with a flow rate of 1 LPM at a 20°C HTF inlet temperature.

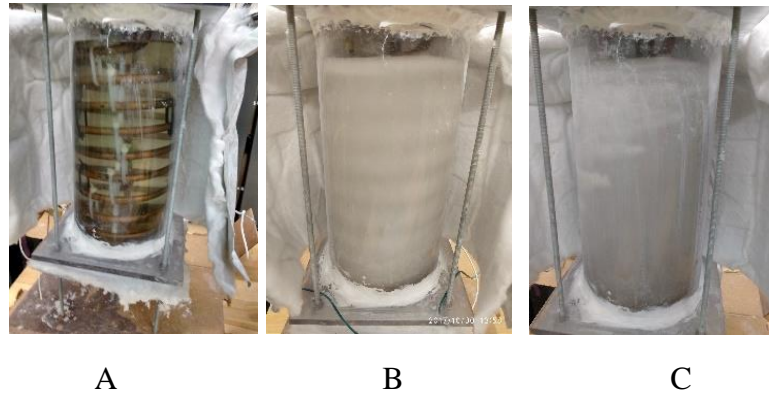


Figure 3.7: Pictures of the discharging test with a flow rate of 1 LPM at 20°C (A: 0 min, B: 30 min, C: 150 min).

3.2.3 The effect of the HTF volume flow rate

The effect of the HTF flow rate on the charging and discharging processes was examined by varying the flow rates for the same inlet HTF temperature. It is seen in Figure 3.8 that increasing the flow rate resulted in the faster melting of the PCM. Faster charging was attributed to the increased forced convection between the HTF and the inner surface of the helical coil, leading to increased heat transfer between the helical coil and PCM (Zhang et al., 2017). This effect was not obvious at the beginning of charging.

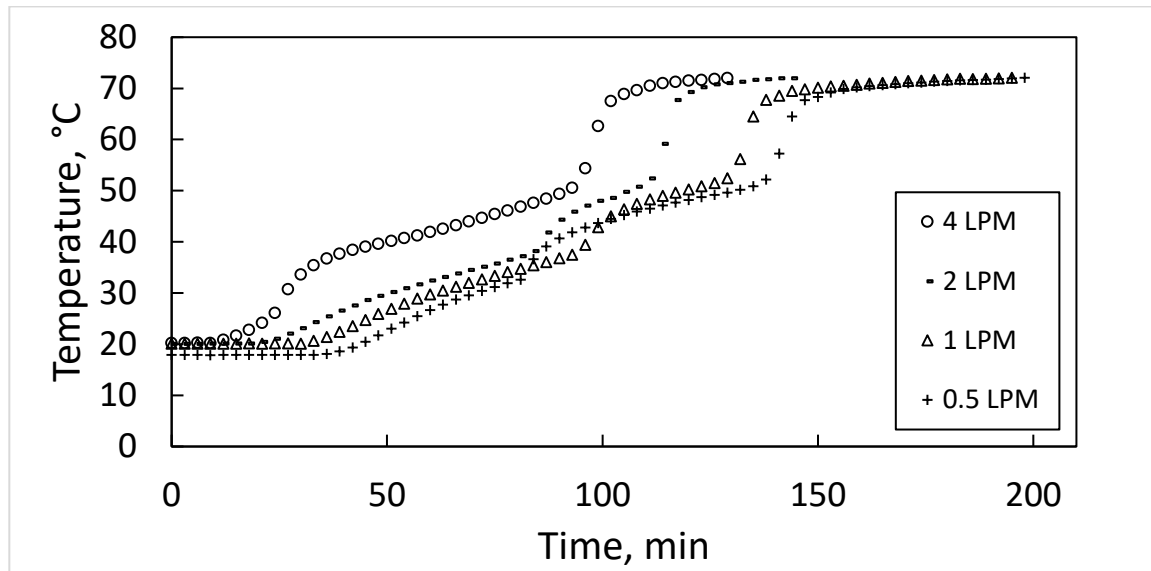


Figure 3.8: Temperature profile of the center top thermocouple at different flow rates during charging at 75°C.

As the melting started and natural convection took control over melting, the temperature increased more quickly due to the increased heat transfer rate. This effect occurred much earlier at a 4 L/min flow rate, showing that the onset of natural convection is expedited at a high flow rate. The total time to attain a temperature of 69°C for all the thermocouples was also measured to compare the charging times at different flow rates for the same HTF inlet temperature (75°C). It is seen from Figure 3.3 that increasing the flow rate from 0.5

L/min to 4 L/min decreased the charging time by 21%. The temperature difference between the inlet and outlet temperature was found to increase with a decreasing flow rate, particularly for the initial charging period.

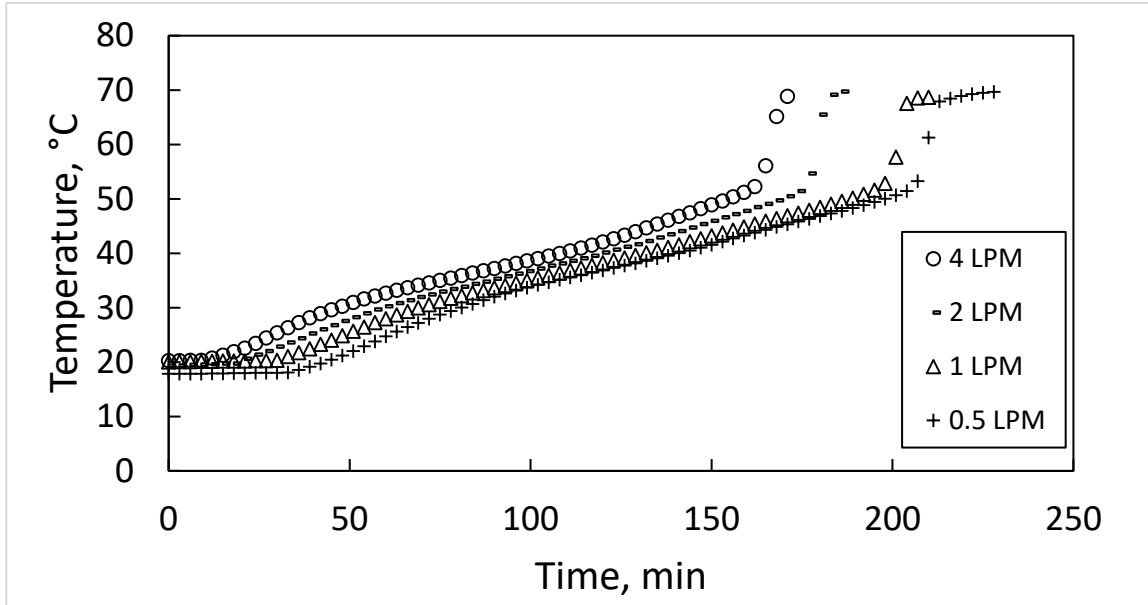


Figure 3.9: Temperature profile of the center bottom thermocouple at different flow rates during charging at 75°C.

As can be seen in Figure 3.9, the temperature increased linearly at the center bottom of the container as this is the last part of the region to be melted. The increased heat transfer at higher flow rates led to a rapid temperature increase.

Figure 3.10 indicates that there was not much change in the temperature profile of the center top thermocouple readings during discharging at different flow rates. A rapid drop in temperature was seen before the PCM went through the liquid-solid transition. After that, the temperature remained at around 55°C for a long time, indicating the liquid-solid phase

change transformation. Upon completion of solidification around 50°C, the temperature decreased almost linearly regardless of the flow rate.

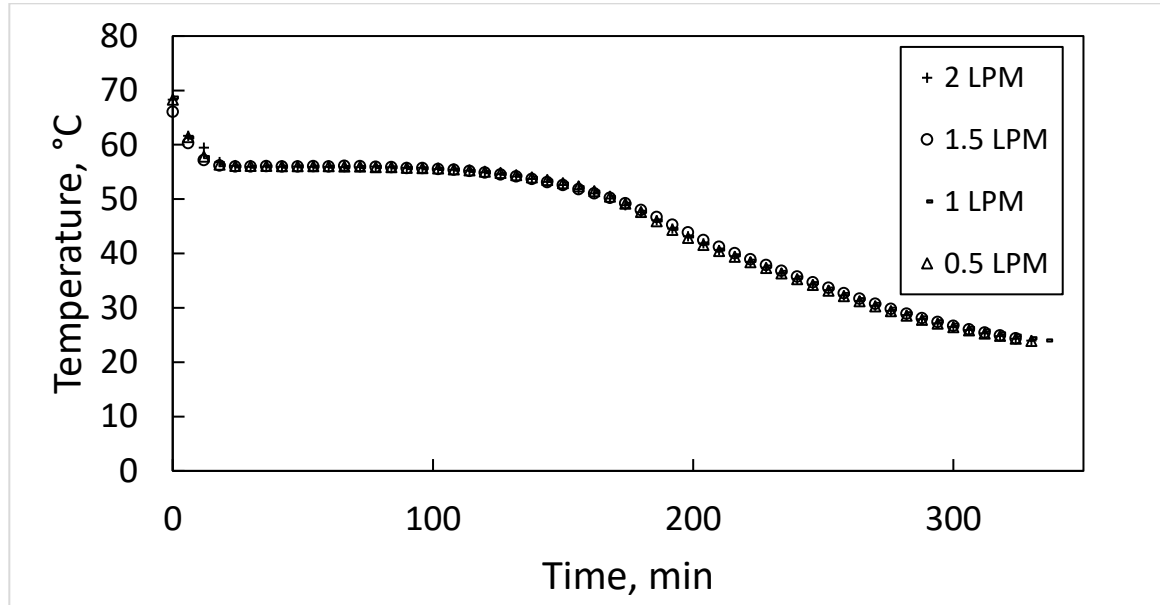


Figure 3.10: Temperature profile of the center top thermocouple at different flow rates during discharging at 20°C

Discharging times for the storage were calculated when all the thermocouples read below 25°C. It was found that discharging took 5 h 32 min for 0.5 L/min while increasing the flow rate to 2 L/min did not reduce the discharging time as depicted in Figure 3.3. This indicates the insignificant impact of the flow rate during discharging. Despite the increased convection heat transfer rate with an increasing flow rate between the HTF and helical coil, the existence of high thermal resistance within the wax prevented this increased heat transfer rate from having any effect on reducing the discharging time, which agrees with previous studies (Sari & Kaygusuz, 2002; Kabbara et al., 2014).

3.2.4 The effect of HTF inlet temperature on charging

The effect of the inlet temperature of HTF on charging time was also investigated. The charging tests were run at 70 and 75°C for the same flow rate (4 L/min). Increasing the inlet temperature from 70 to 75°C reduced the charging time by 35% (Figure 3.3).

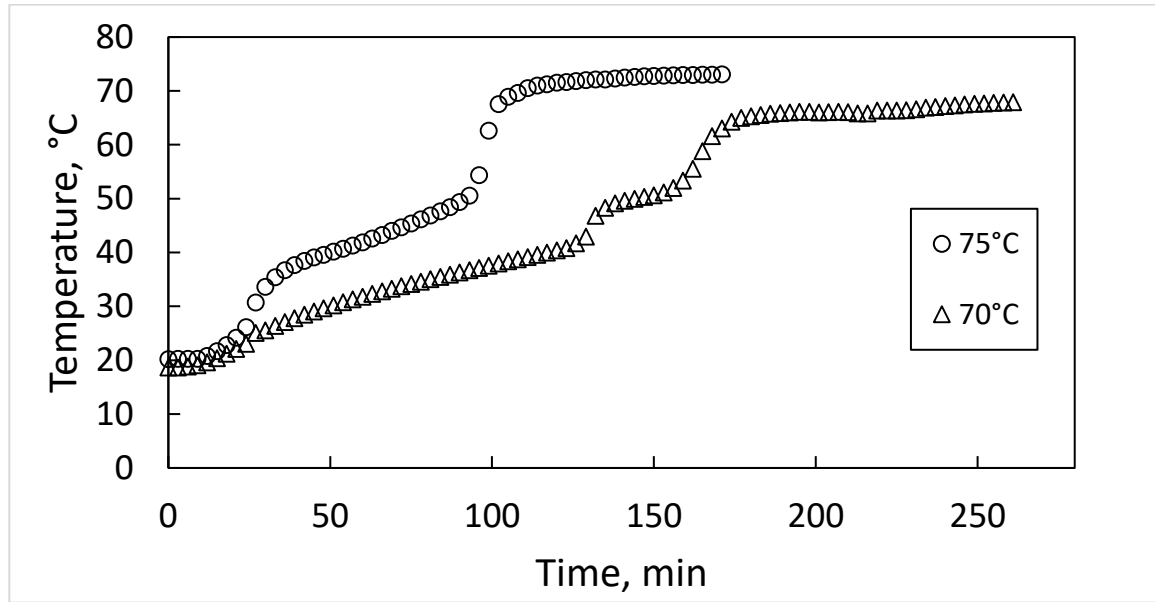


Figure 3.11: Temperature profile of the center top thermocouple at different HTF inlet temperatures with 4 LPM during charging.

It is shown in Figure 3.11 that the temperature increase at the center top thermocouple was identical for both cases at the initial state. However, the higher inlet temperature led to faster melting and triggered the earlier onset of natural convection, which dominated the melting process during charging (Dinker et al., 2017). The temperature increase was found to be more uniform at a 70°C inlet HTF temperature as opposed to separation of the top and middle thermocouples due to the dramatic temperature rise at the 75°C inlet temperature.

3.2.5 The effect of HTF flow direction

Another factor that was investigated during charging and discharging tests were the flow direction of HTF. Previous studies for vertical tube-in-shell configurations showed that upward flow decreases the charging time of the storage due to promoted natural convection effects (Parsazadeh & Duan, 2017).

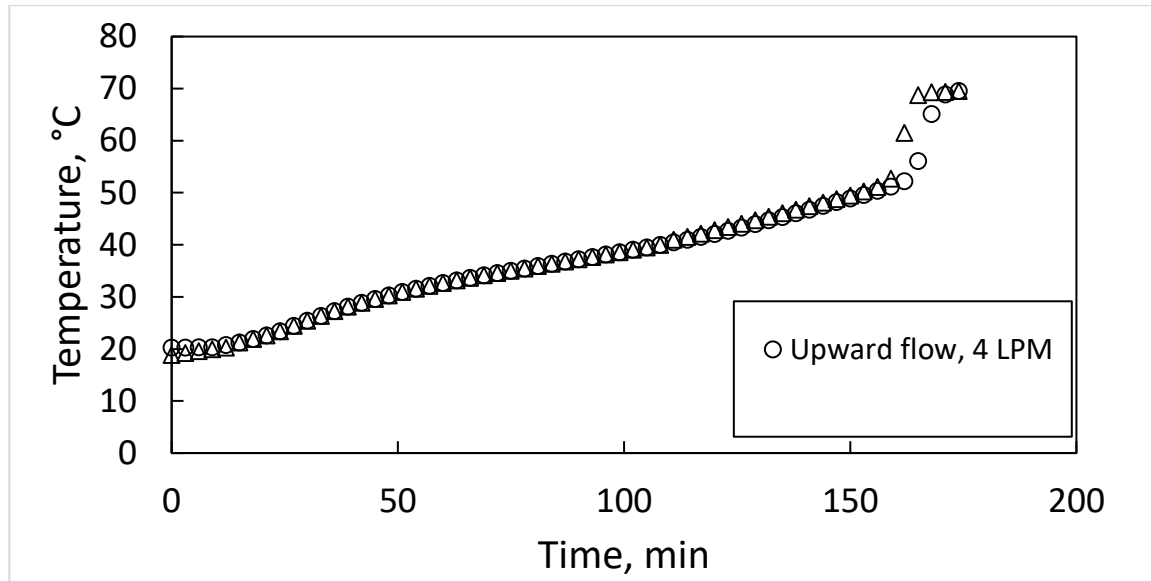


Figure 3.12: Temperature profile of the center bottom thermocouple at different flow directions with 4 LPM during charging at 75°C.

The hotter molten region at the bottom rises due to having lower density for the case of upward flow. This effect has been shown to accelerate melting (Ettouney et al., 2004). However, it is clear from Figure 3.12 that for 4 L/min at 75°C, switching the inlet from the bottom to the top did not lead to longer charging times. This was accounted for by the high flow rate of HTF leading to a uniform temperature along the helical coil. Hence, the flow direction either being downward or upward becomes insignificant for the charging time (Figure 3.3).

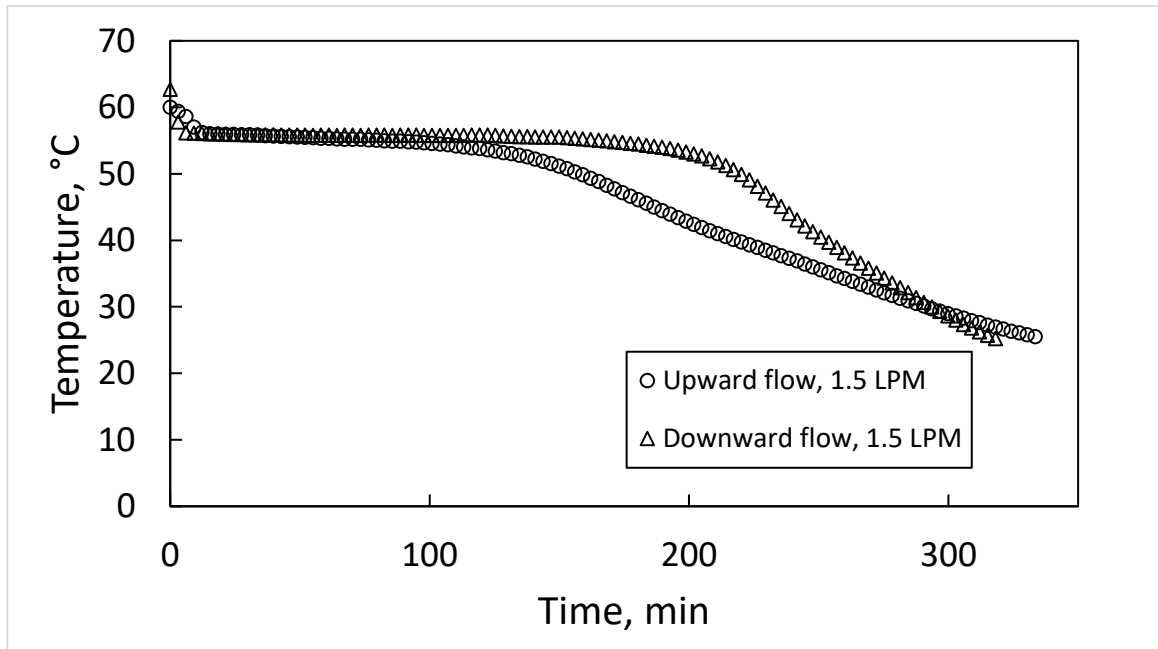


Figure 3.13: Temperature profile of the center bottom thermocouple at different inlet positions with 1 LPM during discharging at 20°C.

As can be seen in Figure 3.13, although the total discharging time did not change notably with switching the flow direction, supplying cold HTF from the top of the container resulted in a longer phase change transition (maintaining the temperature at around 55°C). This might be due to the formation of weak natural convection currents causing the circulation of melted wax when the flow was downward (cooled liquid wax on the top of the storage unit is replaced by the hotter liquid wax rising from the bottom). Therefore, a more uniform temperature distribution was maintained. However, upon completion of the phase change, the PCM temperature at the bottom of the storage unit decreased more quickly compared to the case where cold HTF is supplied from the bottom.

3.2.6 Storage Efficiency

Experimental energy storage efficiency was also determined by finding the instantaneous energy inputs/outputs to the storage using equations (3) and (4). The inlet (T_{in}) and outlet temperature (T_o) readings of the HTF, which were recorded every 20 s (Δt), were used in the calculations. $C_{p,HTF}$ and \dot{m}_{HTF} stand for the specific heat capacity and mass of the HTF, respectively.

$$Q_{supplied} = \Delta t \times \dot{m}_{HTF} \times C_{p,HTF} (T_{in} - T_o) \quad (3)$$

$$Q_{recovered} = \Delta t \times \dot{m}_{HTF} \times C_{p,HTF} (T_o - T_{in}) \quad (4)$$

The recovery efficiency of the storage, η , can also be determined. The ratio of recovered energy from the PCM storage during discharging to the supplied energy to the PCM storage during charging yields the overall recovery efficiency of the storage, which is defined as follows;

$$\eta = \frac{Q_{recovered}}{Q_{supplied}} \quad (5)$$

The recovery efficiency of the storage ranged between 35-62% for the specified discharging flow rates. The highest efficiency was found at a discharging flow rate of 2 L/min, while the lowest efficiency was determined to be 35% for 0.5 L/min. This accounts for the dynamic release of the energy stored in the wax at a higher flow rate. It should be noted that calculations did not consider the heat losses from the storage container to the surrounding environment.

3.3 Summary

This chapter presented the performance of a helical coil latent heat thermal energy storage unit under different operational conditions. Charging and discharging processes were studied by varying the HTF flow rate, HTF inlet temperature and flow direction of HTF. It can be concluded that inlet temperature has a greater impact on the charging time compared to the HTF flow rate. The charging time was reduced by 35% when the inlet HTF temperature was increased from 70 to 75°C. Increasing the flow rate from 0.5 to 4 L/min also reduced the charging time of the storage by 21%, whereas the same effect did not result in any reduction in discharging time. It was found that switching the inlet HTF position from the bottom to the top of the container did not lead to a significant change in charging time. Higher recovery efficiency was achieved at higher flow rates during discharging. A poor heat transfer rate stemming from the low thermal conductivity of the paraffin wax was responsible for the long charging/discharging times. Discharging processes were much longer than charging processes since only conduction exists as the main mode of heat transfer.

Overall, it was seen that heat transfer enhancement techniques are desired to reduce lengthy charging/discharging times. In the following chapter, the dispersion of highly conductive nanoparticles for heat transfer improvement is proposed as a solution to this problem.

Chapter 4 Characterization and Stability Study of NEPCM

This chapter presents the experimental characterization and stability study of paraffin wax as a base PCM with various nanoparticles including MWCNTs, GNPs and Aluminum oxide (Al_2O_3). While most previous studies focused on the thermal conductivity enhancement of NEPCMs, this experimental study is dedicated to the stability issue of NEPCMs after melting/solidification cycles and variation of the thermal conductivity of NEPCMs over time. Comprehensive stability study was conducted to address stability issues along with thermal conductivity enhancement. A DSC study was also undertaken to investigate the effect of nanoparticles' presence on the phase change temperature and latent heat capacity of paraffin wax.

4.1 Materials and Methods

4.1.1 Materials

All the materials including nanoparticles, base PCM and surfactants were purchased from Sigma Aldrich. Paraffin wax has a phase change temperature of 53-57°C. MWCNTs have the following parameters: 6-9 nm in diameter and 5 μm in length. The Al_2O_3 nanoparticles have less than a 50-nm particle size and GNPs have lateral dimensions of about 2-3 μm as specified by the manufacturer. Sodium oleate and Octadecylamine were used as surfactants to promote long-term stability. Figure 4.1 shows pictures of the materials.

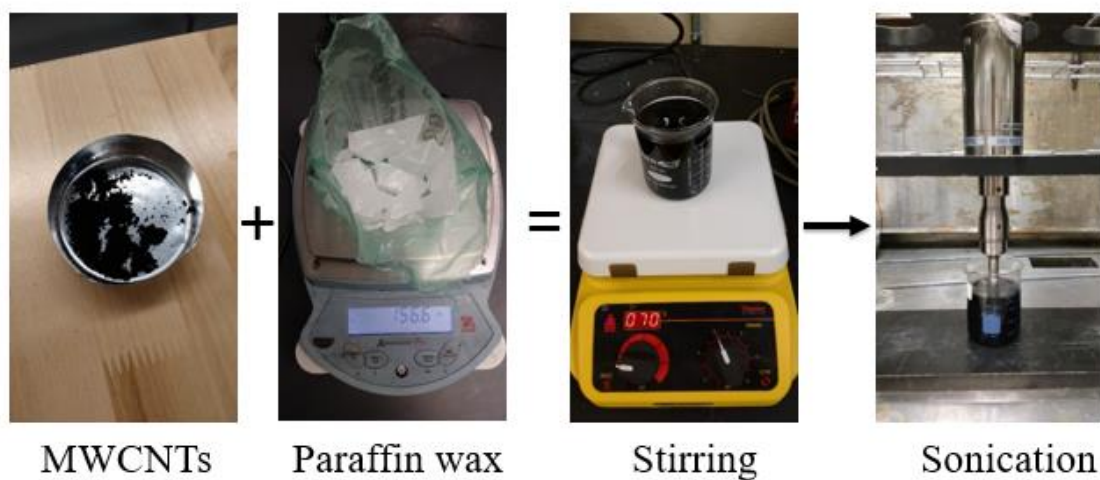


A B C D E F

Figure 4.1: A: Paraffin wax, B: MWCNTs, C: Al_2O_3 , D: GNPs. E: Sodium oleate, F: Octadecylamine.

4.1.2 Sample preparation

NEPCM preparation is a gray area where many researchers tend to use their own “recipe”, as the preparation methods lack universal established standards (Michaelides, 2014). Certain guidelines are necessary to obtain consistent and reliable NEPCMs. That said, the variety of base PCMs and nanoparticles makes it difficult to come up with a standardized preparation.



MWCNTs Paraffin wax Stirring Sonication

Figure 4.2: Sample preparation using the mechanical dispersion method.

In this study, the first batch of samples was prepared with only the mechanical dispersion method. A desired amount of each nanoparticle corresponding to 0.5, 1 and 2% by mass and paraffin wax were first weighed on electronic scales (Denver Instrument-Model P-214, Ohaus Corporation-Adventurer Pro AV8101C, respectively). Then, paraffin wax was melted in a beaker on a hot plate stirrer (SP131320-33Q, Cimarec - Thermo Scientific). The temperature of the hot plate stirrer was kept above the melting temperature at 70°C. Magnetic stirring was applied for 1 h at an average speed of 600 rpm after adding the specified amount of nanoparticles. Stirring was followed by sonicating the samples for an hour at 30% amplitude (50 W, Sonifier Cell Disrupter, Branson). Figure 4.2 shows the sample preparation process.

The second and third batches of samples were prepared with Sodium Oleate and Octadecylamine surfactants, respectively. The previous NEPCM preparation procedure was followed. The only difference was that surfactants were added during stirring. Sodium Oleate with a mass ratio of 1:10 to nanoparticle amount was selected while the Octadecylamine to nanoparticle mass ratio was chosen as 2.5:1 following Tang et al. (2014).

4.2 Thermal Conductivity Measurements

Thermal conductivity measurements were taken using a KD2 PRO Thermal Conductivity Analyzer (Decagon Devices, USA). This probe has been widely used in previous studies (Ho & Gao, 2009; Jesumathy et al., 2011; Cui et al., 2011; Yu et al., 2012; Kumaresan et al., 2012; Mehrali et al., 2013; Fan et al., 2013; Lokesh et al., 2015). The measurement technique is based on the transient-line-heat-source theory. In this theory, a known amount

of current is passed through an infinitely long and very thin line which is buried in a semi-infinite medium. The line source acts as a temperature sensor and a heat dissipater. Depending on the thermal conductivity of the medium, the temperature of the probe increases rapidly or slowly (the lower the thermal conductivity of the medium, the higher the temperature increase). Using this temperature response, the thermal conductivity is determined (Paul et al., 2010). KD2 Pro has three sensors specifically designed for different materials (Fig. 4.3). The KS-1 sensor, which is 6.1 cm in length and 1.3 mm in diameter, can only be used for liquids and insulation materials. Its measurement scale ranges from 0.02 to 2 W/m·K with an accuracy of $\pm 5\%$. The main issue regarding the thermal conductivity measurement of liquids is the presence of free convection. To address this problem, the sensor should be used in a low power mode with a minimum measurement time, which can be set to a minute. The sensor should also be still during measurement and any kind of vibrations due to ventilation, fans, or movements in the lab should be avoided. In addition, needle alignment plays an important role in measurements. Thus, even a slightly angled needle may lead to an error.

A TR-1 sensor is used for granular and porous materials. It has a bigger needle (10-cm long, 2.4-mm diameter). The larger size results in longer heating times to eliminate the contact resistance in granular samples or solid samples with pilot holes. It applies more heat during measurement than the KS-1 sensor. It has a greater range of measurement, from 0.1 to 4 W/m·K with higher uncertainty $\pm 10\%$. The dual SH-1 is another sensor that measures volumetric capacity, thermal diffusivity, thermal diffusivity and thermal

resistivity along with thermal conductivity. It also has a range of 0.2 to 2 W/m·K with an accuracy of $\pm 10\%$ for thermal conductivity (Decagon Devices, 2011).

For this study, the KS-1 sensor was used for liquid phase measurements while the TR-1 sensor was found to be more compatible with solid NEPCM and therefore was used. Before the measurements, the sensors were calibrated with the standard materials provided by the manufacturer.



Figure 4.3: KD2 Pro Thermal Conductivity Analyzer and its sensors: TR-1, KS-1, SH-1 (from left to right).

4.2.1 Monitoring the thermal conductivity of NEPCMs in liquid phase

Samples in liquid phase were taken to the environmental chamber and thermal conductivity measurements were first conducted in liquid phase at 70°C within the first hour after sample preparation. Then, the temperature was set to 60°C and continuous thermal conductivity measurements were repeated at that temperature hourly, as shown in Figure 4.4. The main purpose of this test is to observe if there is any change in thermal conductivity due to sedimentation and nanoparticle instability over time.

The results in Figure 4.4 showed a range of 0.15 to 0.17 W/m·K for the thermal conductivity of paraffin wax in liquid phase at 60°C with different nanoparticles. The settlement of most nanoparticles occurred when thermal equilibrium was reached after a sufficient time. This caused the overall trend of thermal conductivity to decrease with time for the NEPCMs. Compared with paraffin wax, all NEPCMs showed an insignificant increase of thermal conductivity due to the agglomeration and sedimentation of nanoparticles (pictures in the next sections) and thus not providing the required nanoparticle network within the measurement region. The thermal conductivity of MWCNT-wax samples was lower than that of GNP and Al₂O₃-wax samples due to the complete settlement of nanoparticles in the former.

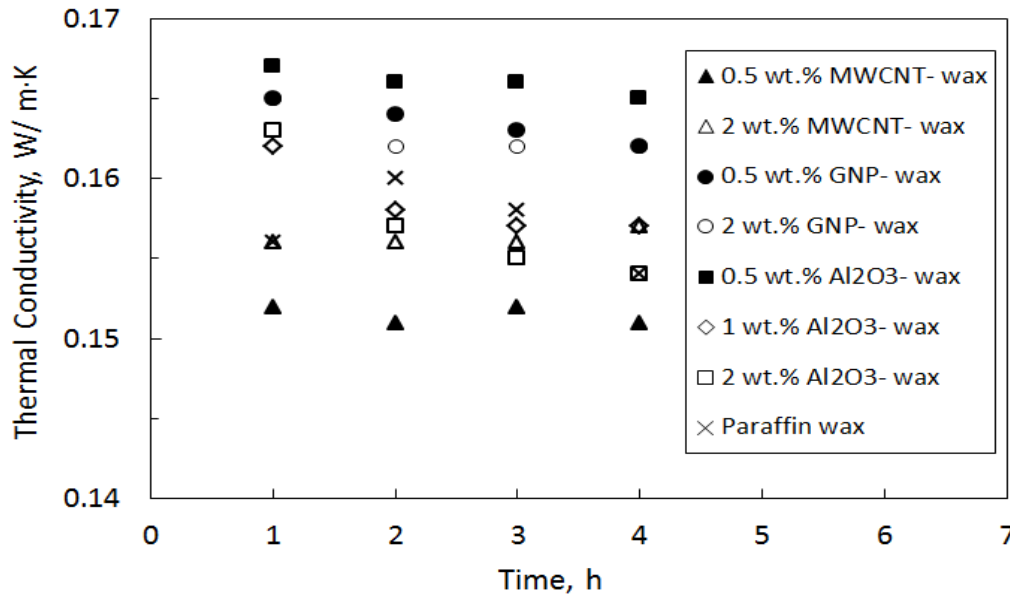


Figure 4.4: Thermal conductivity change in liquid phase (60°C) over time after sample preparation.

4.2.2 Thermal conductivity change of NEPCMs with temperature

After the measurements were done in liquid phase, the samples were poured into a mold designed for solid phase measurements. The mold was printed using a 3-D printer to create a pilot hole in the sample during solidification (Figure 4.5). Once the samples were fully solidified at ambient temperature, measurements were conducted in the thermal chamber at 25, 35 and, 45°C. The pictures of solid samples can be seen in Figure 4.6.

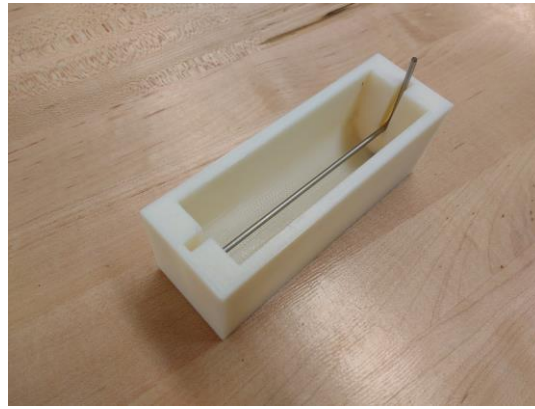


Figure 4.5: 3-D printed mold for thermal conductivity measurements in solid phase.

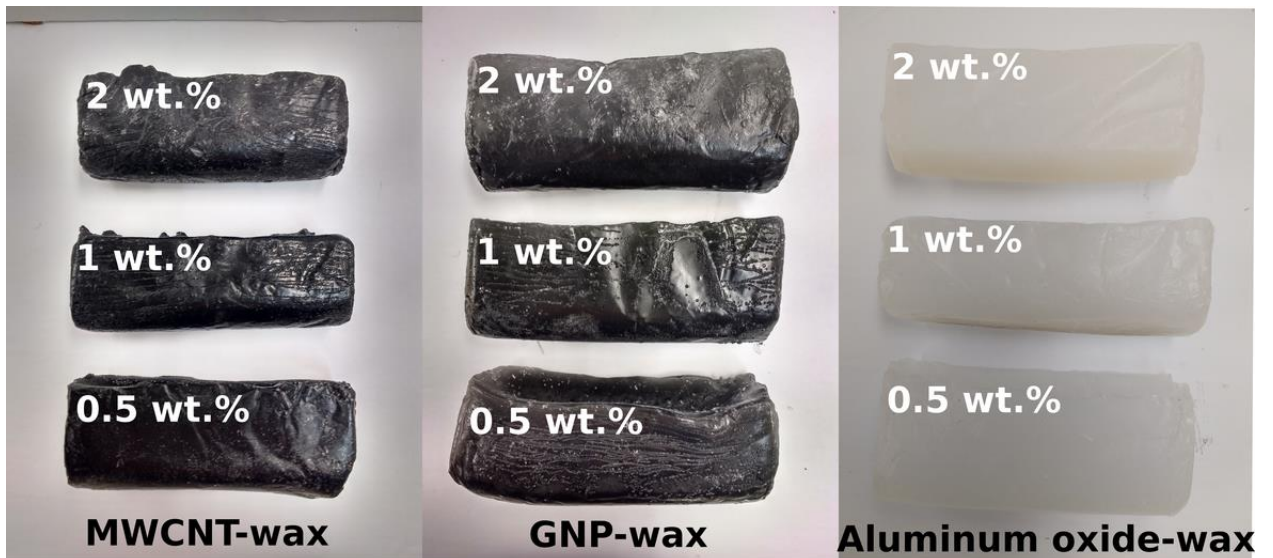


Figure 4.6: Picture of each sample after being removed from the mold.

Figure 4.7 revealed that thermal conductivity ranges from 0.15 to 0.16 W/m·K for paraffin wax with different concentrations of MWCNTs in liquid phase. It was seen that samples were highly viscous with mud-like texture as the MWCNTs content increased from 0.5 to 2 wt.%. This could deteriorate the natural convection induced melting. Solid phase measurements exhibited temperature dependency where thermal conductivity peaked at 35°C for all the concentrations possibly due to the solid-solid transition (Wang et al., 2009; Tang et al., 2014). During the transition, the crystal structure changes might have affected how energy is transferred between solid particles (molecular view of heat conduction and thermal conductivity). The highest enhancement was achieved for 2 wt.% MWCNT-paraffin wax by 13% at 35°C (Figure 4.7). Overall, no significant improvement in thermal conductivity was observed with the addition of MWCNTs. In some cases, the presence of MWCNTs deteriorated thermal conductivity, possibly due to highly entangled bundles of nanotubes (Wu et al., 2016).

GNPs were expected to increase the paraffin's thermal conductivity significantly. Hence, initial measurements right after sample preparation within the first hour showed that thermal conductivity increased sharply for all the concentrations. It should be noted that results at 70°C showing a good thermal conductivity enhancement from 0.15 to 0.21 W/m·K were believed to be caused by considerable uncertainty in measurements due to natural convection and particle motion at that high a temperature (Figure 4.8). However, the addition of GNPs to wax increased the thermal conductivity only marginally ranging from 0.16-0.17 W/m K at 60°C. This was because of the sedimentation of the majority of GNPs when thermal equilibrium was reached after a sufficient time.

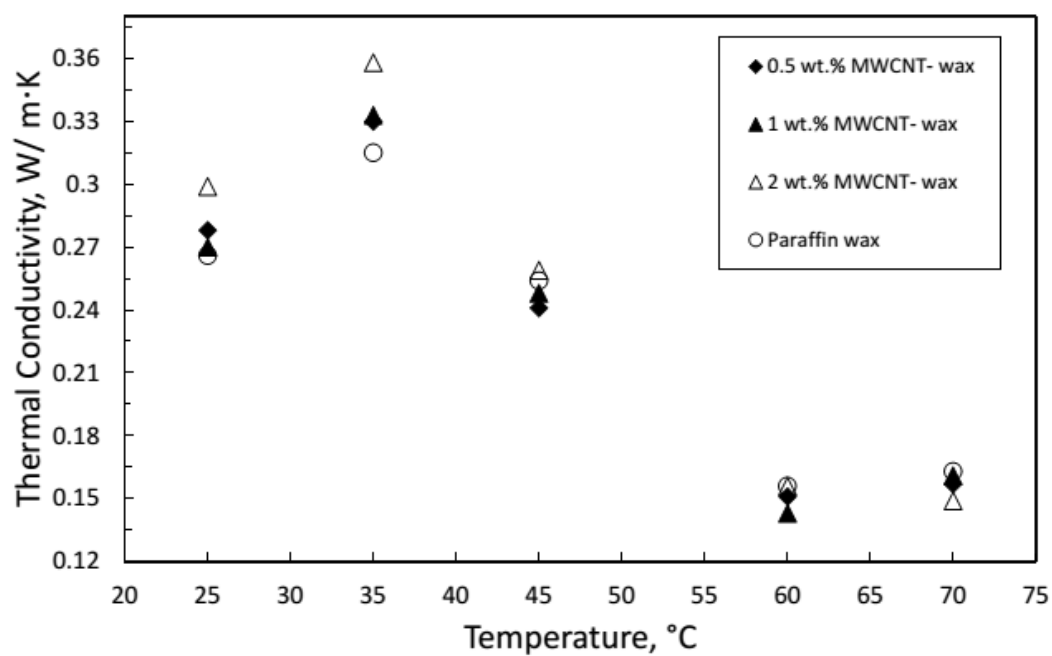


Figure 4.7: Thermal conductivity change of MWCNT-wax samples with temperature.

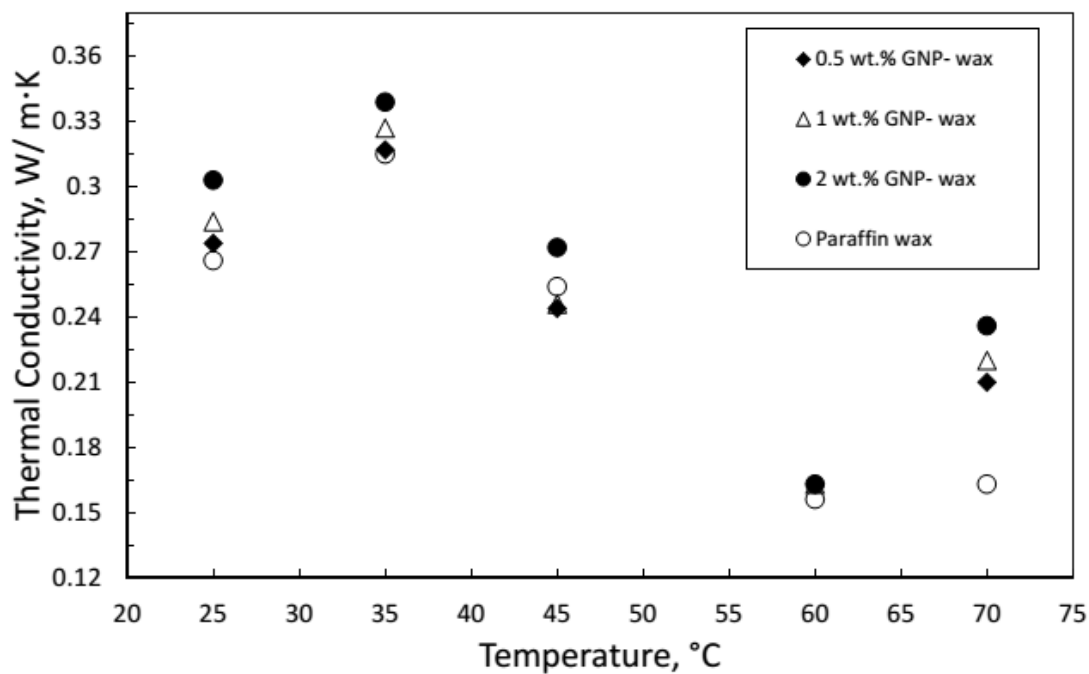


Figure 4.8: Thermal conductivity change of GNP-wax samples with temperature.

After liquid phase measurements, samples were poured into the mold. It was observed that the majority of particles were stuck on the bottom surface, proving the settlement of particles. Therefore, it could be said that measurements for GNPs doped paraffin wax do not really represent the actual nanoparticle content of the samples. Only a small fraction of particles that were dispersed into the wax were scattered, slightly improving the thermal conductivity. Thus, the accuracy of measurements is questionable due to the instability of GNPs in paraffin wax. Increasing nanoparticles linearly did not lead to proportional enhancement in thermal conductivity. Particle settlement played an important role in not providing the desired enhancement. This is more evident in solid phase, where measurements were made at 25, 35 and 45°C. It was seen that increasing the GNP content led to a minor increase. This is also attributed to the reduced GNP content due to not being able to transfer the particles that get stuck on the bottom surface into a mold.

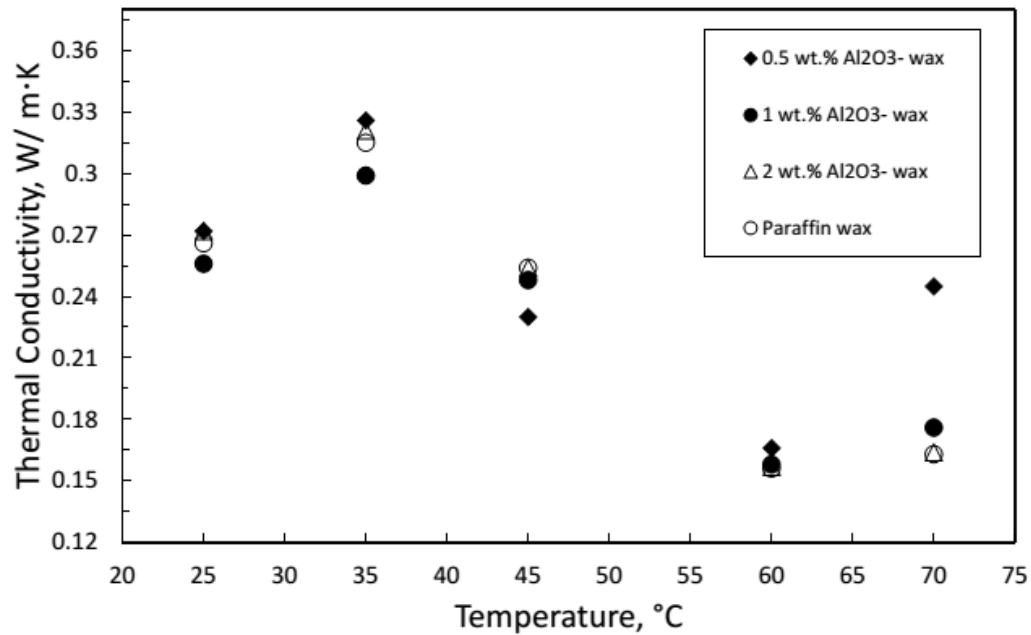


Figure 4.9: Thermal conductivity change of Al₂O₃-wax samples with temperature.

The presence of Al_2O_3 nanoparticles also slightly enhanced the thermal conductivity. This enhancement, however, was not proportional to the nanoparticle increase. Lower loadings of Al_2O_3 resulted in higher enhancement in the liquid phase, even with an outlier at 70°C for 0.5 wt.% Al_2O_3 due to natural convection possibly induced by Brownian motion (Figure 4.9). The precipitation issue again affected the measurements. It was seen that particles started to settle immediately once sonication was completed. Therefore, it was not possible to evaluate the potential of nanoparticles based on the obtained data. Solid phase measurements also revealed biased results, mainly fluctuating within the vicinity of pure paraffin wax's thermal conductivity without any clear trend. It was also seen that there was just a small change in thermal conductivity with a mild decrease for the measurements that were done an hour after sample preparation (Figure 4.4). This is possibly due to already-deposited particles within the first hour.

4.3 Differential Scanning Calorimetry (DSC) Measurements

DSC study was carried out to determine the melting/solidification temperatures and latent heat capacity of paraffin wax nanocomposites. The DSC equipment (Mettler-Toledo DSC1, Differential Scanning Calorimeter) is shown in Figure 4.10. Figure 4.11 shows the heating and cooling curves of the samples with a heating/cooling rate of $5^\circ\text{C}/\text{min}$. Two distinct peaks can be seen on both the heating and cooling curves, where the smaller peak corresponds to the solid-solid transition at around 35°C and the larger peak indicates the solid-liquid transition at around $50\text{-}55^\circ\text{C}$.

The peak temperatures of pure paraffin wax for melting and solidification were found to be 54.86 and 53.02 °C, respectively (Table 4.1). This demonstrates an insignificant supercooling of 1.84°C. The presence of nanoparticles seemed to increase the melting

Table 4.1: DSC results of NEPCM samples ($T_{m,peak}$: peak melting temperature, $T_{s,peak}$: peak solidification temperature, ΔT : supercooling, ΔH_m : enthalpy of solid-liquid transition during melting, ΔH_s : enthalpy of solid-liquid transition during solidification).

Samples	$T_{m,peak}$ (°C)	$T_{s,peak}$ (°C)	ΔT (°C)	ΔH_m (J/g)	ΔH_s (J/g)
Paraffin wax	54.86	53.02	1.84	124.6085	126.8456
0.5 wt.% MWCNT-wax	54.09	52.95	1.14	127.5281	124.7191
1 wt.% MWCNT-wax	52.72	53.1	-0.38	130	127.1875
2 wt.% MWCNT-wax	54.77	52.15	2.62	120.3365	120.8109
0.5 wt.% Graphene-wax	56.18	52.17	4.01	114.7383	112.2494
1 wt.% Graphene-wax	56.18	52.17	4.01	133.8488	134.1877
2 wt.% Graphene-wax	55.88	52.44	3.44	115.3103	114.5671
0.5 wt.% Aluminum oxide-wax	56.19	53.76	2.43	138.1738	136.1664
1 wt.% Aluminum oxide-wax	56.19	51.94	4.25	94.29853	93.62517
2 wt.% Aluminum oxide-wax	55.33	52.4	2.93	117.2595	116.3339

peak temperatures by 1-2°C, except for MWCNT-wax samples, while the freezing peak temperature was reduced with the same effect except for the 0.5 wt.% Al_2O_3 -wax sample.

The supercooling issue became worse with the addition of nanoparticles reaching up to 4.25°C except for 0.5 and 1 wt.% MWCNT-wax samples. This unusual behavior contradicts the common belief that nanoparticles reduce the supercooling issue by acting as a nucleating agent (Wang et al., 2009; Tang et al., 2014; Wu et al. 2015).

Phase change enthalpies were also found to be 124.61 and 126.84 J/g for pure paraffin during melting and freezing curves, respectively. Nanoparticle addition had different

effects on the phase change enthalpies. A varying degree of decrease in enthalpies was seen for all the nanoparticle-wax samples at the highest concentration (2 wt.%). However, the trend for other concentrations was somewhat unclear with random increases and decreases.



Figure 4.10: Mettler-Toledo DSC1, Differential Scanning Calorimeter.

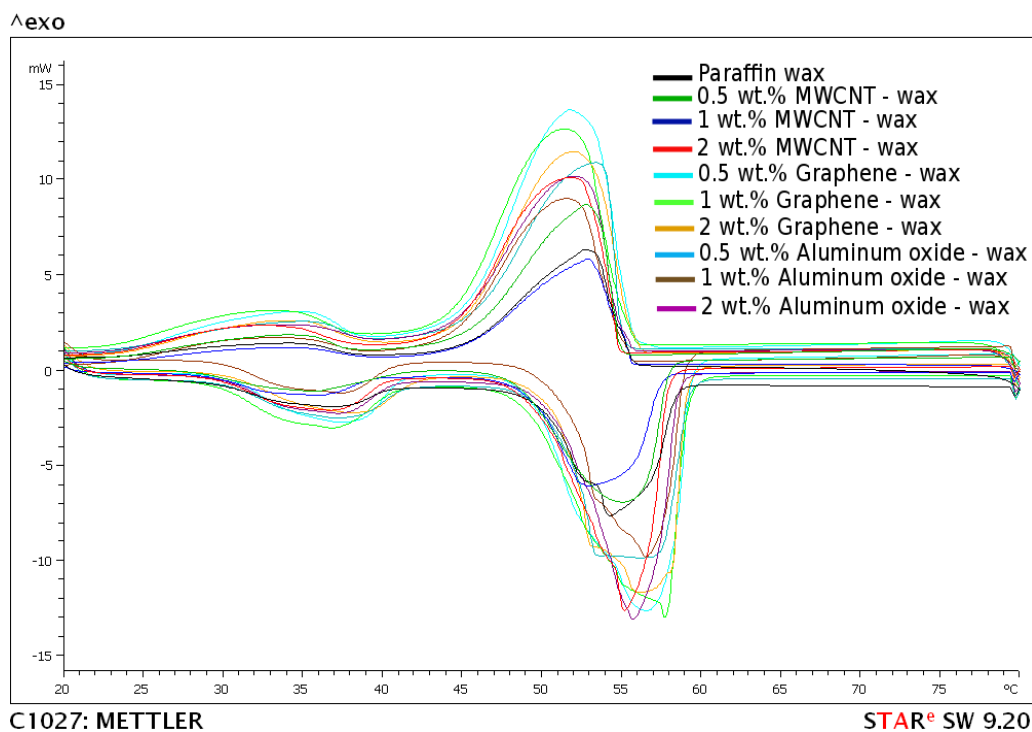


Figure 4.11: DSC heating and cooling curves of paraffin wax with MWCNT, GNP and Al_2O_3 nanoparticles at different concentrations.

One would expect lower latent heat (enthalpy change) when nanoparticles are added to a pure PCM since the particles will not contribute to latent heat. For the unusual increase of latent heat seen in the measurements, two causes are believed to be possible, one is related to the measurement uncertainty within the DSC instrument; the other more important one is related to the stability issue. The samples in DSC measurements were cut from different parts of a larger composite sample (in which nanoparticles could have deposited to one edge). The nanoparticle concentrations used in our analysis were therefore not reliable.

4.4 Stability of Paraffin Wax with Nanoparticles

In the evaluation of the stability of NEPCMs, sedimentation observation was selected. There are plenty of reasons for choosing this method. Firstly, the relatively high melting temperature of the paraffin wax (53-57°C) restricts the usage of optical spectroscopy methods since there is no temperature control on the samples during measurements. Second, the observation of stability over consecutive thermal cycles is not practical with these methods due to solid-liquid phase change and the transparency issue. In addition, the zeta potential method is not suitable due to the non-polar characteristics of paraffin wax. It can be said that the optical spectroscopy methods provide a better option for nanofluid stability while visual stability evaluation is thought to be the most suitable method for NEPCMs.

4.4.1 Effect of sonication on the stability of mechanically-prepared NEPCM

One of the objectives of this study was to investigate the effects of sonication time on the stability of samples. To do that, melting-solidification thermal cycles for MWCNT-wax NEPCMs were performed in the environmental chamber (25 - 80°C). To avoid adverse

effects of high viscosity caused by high MWCNTs concentrations, lower fractions (< 0.1 wt.%) were examined. After each cycle, pictures of the samples were taken in liquid phase to assess the uniformity and homogeneity of nanoparticle dispersion. Figure 4.12 shows these pictures with different sonication times and different MWCNT loadings in the wax over three thermal cycles.

A thin layer of a particle-free region can be observed after the first thermal cycle in Figure 4.12-(1). Accumulated MWCNT clusters started to settle at the bottom of the containers. As a result, the particle-free regions in the last two cycles grew substantially as shown in Figure 4.12 (2-3). After the third thermal cycle, up to a certain height from the bottom of the container, samples have a dark color indicating highly agglomerated nanoparticles. However, transparent regions on the upper portion indicated that there was no particle network there. The higher density of the clustered MWCNT may have led to their settlement on the lower portion.

Sonication duration time did not seem to have any effect on the dispersion quality of MWCNTs in the wax. Also, settlement and clustering were evident over thermal cycles regardless of MWCNT fractions. The results indicated that mechanical dispersion through stirring and sonication is not sufficient to change interfacial forces between the nanoparticles and the paraffin wax for long terms. Therefore, well-dispersed colloidal systems were not sustained. It should be noted in Figure 4.12-(2) that samples D and E appeared to have good dispersion after the second cycle, but this was due to the replacement of broken beakers. However, samples D and E followed the same trend as samples A, B and C in terms of particle settlement as is obvious after the third thermal cycle as shown in Figure 4.12-(3). Fig 4.13 also presents the degree of settlement for the MWCNT-wax sample in solid phase.

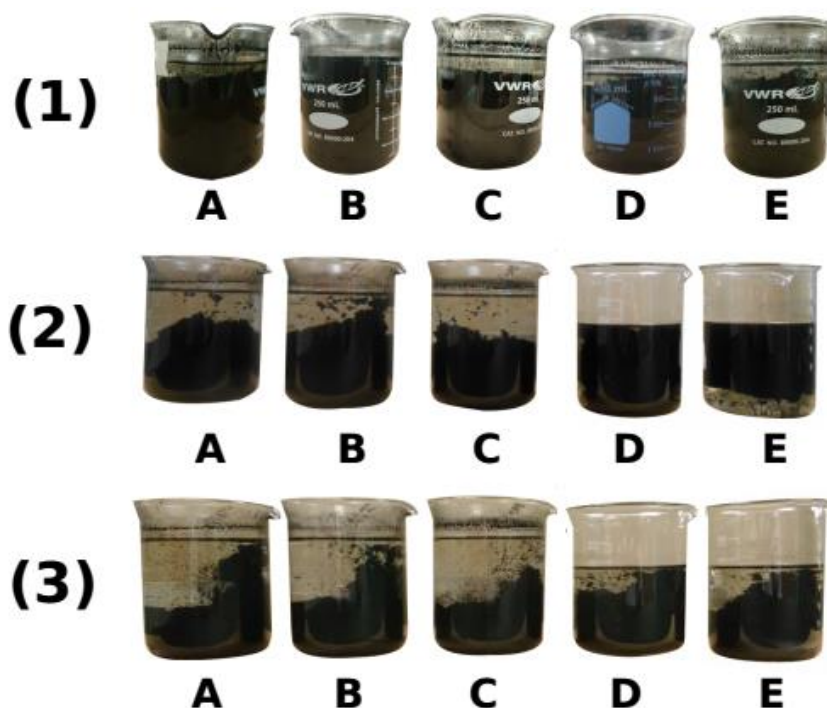


Figure 4.12: Stability observation of MWCNT-wax samples in liquid phase over the first (1), second (2) and, third (3) melting/solidification cycles (Sample A: 0.1 wt.%, 100 min sonication; B: 0.1 wt.%, 40 min sonication; C: 0.075 wt.%, 70 min sonication, D: 0.05 wt.%, 100 min sonication, E: 0.05 wt.%, 40 min sonication).



Figure 4.13: Settling of MWCNTs in paraffin wax.

4.4.2 Effectiveness of surfactants on the stability of NEPCM

The results above demonstrate that mechanical dispersion methods (stirring and sonication) are not sufficient to achieve the long-term stability of paraffin wax-based NEPCMs. Surfactants were then investigated for NEPCM preparation. Melting-solidification thermal cycles were performed between 25-80°C in the environmental chamber again to see the effect of sodium oleate as a surfactant.












#C	Liquid Phase	Solid Phase
0		
1		Broken beakers
2		
3		
4		
5		

Figure 4.14: Stability observation of different types of nanoparticles in paraffin wax with sodium oleate as a surfactant in NEPCM preparation, #C represents the number of melting/solidification cycles.

Images captured after each cycle are shown in Figure 4.14 both in solid and liquid phases. Pictures of samples right after preparation (#C=0) were also included.

Unlike the GNP-wax (Figure 4.11 – left beaker in each cell) and Al_2O_3 -wax samples (middle beaker in each cell), the stability evaluation for MWCNT-paraffin wax composite was far more distinct thanks to the dark color of the MWCNT (right beaker in each cell). The MWCNT within paraffin were uniformly dispersed and relatively stable after sample preparation in liquid phase (pictures labeled as 0). However, a thin, particle-free region emerged in the second thermal cycle. Later, the MWCNT-paraffin wax sample was subjected to further thermal cycles. As a result, larger particle-free layers formed on the upper portion of the beakers, with the MWCNT settling at the bottom of the container. The gradual deterioration of dispersion is apparent in both liquid and solid phases for MWCNT-paraffin wax samples.

It was challenging to assess the stability of Al_2O_3 -wax samples in solid phase due to the similar colors of the wax and nanoparticles. However, it was noticed that the majority of white Al_2O_3 nanoparticles precipitated at the bottom of the container, even after the first thermal cycle in liquid phase. Only a small number of nanoparticles were suspended within the wax medium. A closer look at the sample revealed that the fraction of particles suspended in paraffin wax decreased as the Al_2O_3 -wax sample experienced thermal cycles. GNP dispersion in the wax was better compared to MWCNT and Al_2O_3 nanoparticles. In liquid phase, GNP nanoparticles seemed to maintain their uniform dispersion over thermal cycles. However, when the samples were solidified after each cycle, graphene nanoplatelets were seen to have settled on the bottom of the container.

Realizing that Sodium Oleate did not help much in improving the nanoparticle dispersion in the wax, a new batch of samples was prepared with Octadecylamine as a surfactant. The same procedure was followed to perform the stability evaluation. Figure 4.15 shows images of the NEPCM after each cycle. The precipitation did not take place upon solidification of the samples right after sample preparation at room temperature. However, the stability of NEPCM degraded over thermal cycles for all three types of nanoparticles.

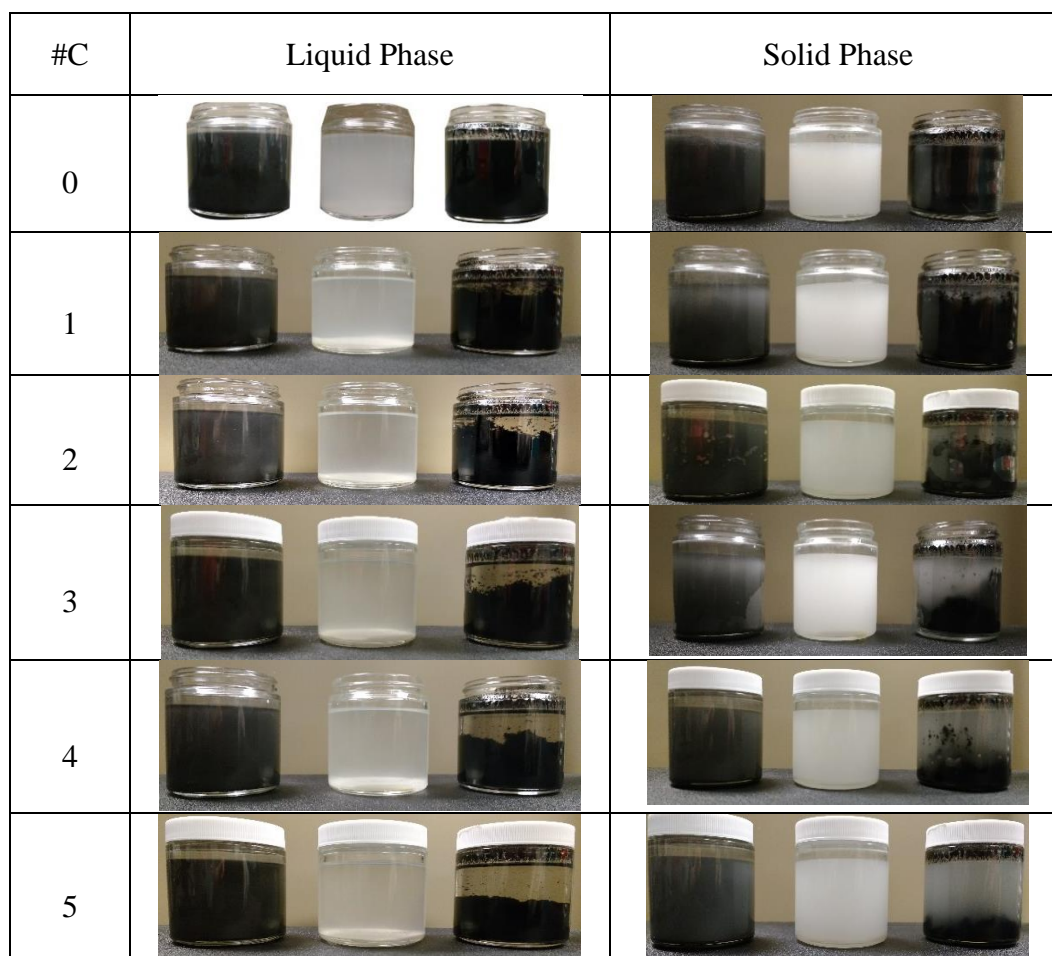


Figure 4.15: Stability observation of various NEPCM prepared with octadecylamine

There are several possible reasons for the ineffectiveness of these surfactants in this paraffin wax-based NEPCM. The fundamental reason is related to the chemical nature of the PCM

and nanoparticles: the wax has nonpolar molecules, while the nanoparticles have polar ones. The surfactants may be able to alter the intermolecular forces for a short period of time. However, they may not be able to sustain through multiple solidification-melting cycles. Other possible reasons could include the surfactants not being able to achieve their critical micelle concentration (CMC) and the inadequate pH value of the solutions (Hormozi et al., 2016; Das et al., 2008, Butt et al., 2003). Unfortunately, these chemical details are beyond the scope of this mechanical engineering research.

4.4.3 Effect of boundary conditions on stability

Boundary conditions during heating and cooling may affect the dispersion quality of nanoparticles within NEPCM. The results shown above were from thermal cycles in an environmental chamber. A different boundary condition during melting and solidification was investigated by placing NEPCM samples on a hot plate at 150°C for melting and leaving the sample at ambient room temperature for solidification. It was thought that heating from the bottom of the samples during melting might help prevent the settlement of nanoparticles due to induced natural convection. New samples were prepared following the previous dispersion method using the same concentration of MWCNT (0.1wt.%) with octadecylamine (1:10 ratio to nanoparticle) as a surfactant.

Heating the samples from the bottom indeed helped in preventing MWCNTs from settling. The constant motion of particles with natural convection was apparent during the heating period. As can be seen from Figure 4.16, the samples seemed stable after melting on the hot plate for 2 h. There was no separation between MWCNTs and wax in liquid phase due to the promoted natural convection after each cycle. Within the first two thermal cycles, nanoparticles appeared to be well dispersed even in solid phase. However, agglomerated

regions started to form with the onset of solidification during the 3rd thermal cycle. The settlement of nanoparticles became worse in later thermal cycles.

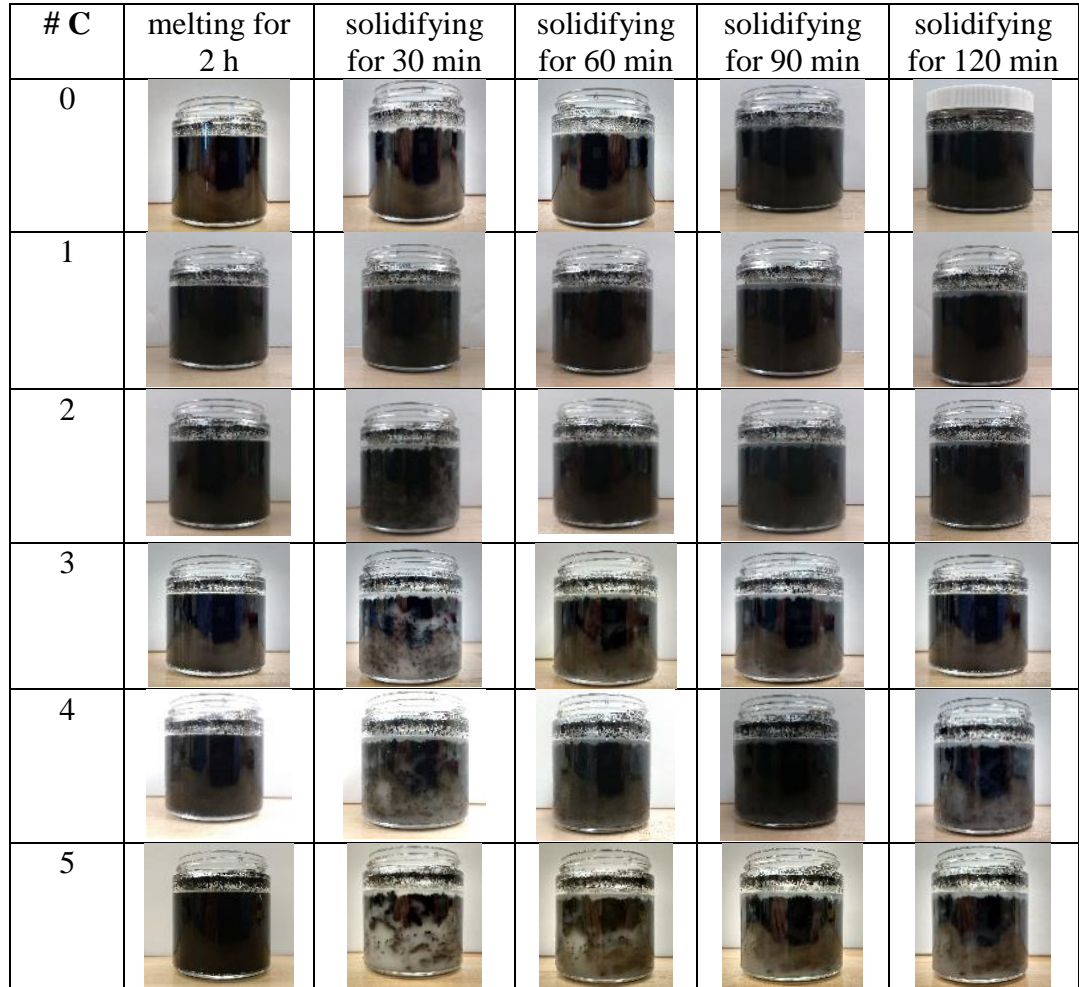


Figure 4.16: Solidification of a 0.01wt.% MWCNT-wax sample after melting on a hot plate at 150°C.

4.5 Summary

Chapter 4 showed the results of the characterization and stability study of paraffin wax with MWCNTs, GNPs and Al₂O₃ nanoparticles. Some of the significant findings can be summarized below:

- The highest thermal conductivity enhancement by 13% was obtained for a 2 wt.% MWCNT-wax sample at 35°C. The insignificant overall improvement of thermal conductivity was due to the particle agglomeration and settlement associated with poor dispersion quality.
- Mechanical dispersion methods were not sufficient to achieve the long-term stability of MWCNT-dispersed NEPCM.
- DSC study showed that, contrary to common belief, the presence of nanoparticles degraded the supercooling issue. However, it should be kept in mind that the stability issue along with the very small sample used during the DSC affected the measurements. Therefore, the results did not certainly represent the properties of NEPCM samples in bulk.
- Paraffin wax-nanoparticle samples became unstable and settled after thermal cycles regardless of the heating method, sonication time, and surfactant usage (sodium oleate, octadecylamine).

Chapter 5 Conclusions and Recommendations

5.1 Conclusions for Experimental Study of LHTESS with Paraffin Wax

The use of latent heat of PCMs in thermal energy storage holds great importance. The first part of the thesis evaluated the performance of a helical coil latent heat energy storage unit with paraffin wax as a phase change material. The charging and discharging characteristics were examined under different operational conditions. The following conclusions are drawn from the results of the experiments:

- 1) Among the operating parameters, HTF inlet temperature had the greatest effect on the charging time of the storage unit. The increase of the HTF inlet temperature from 70°C to 75°C resulted in a reduction in charging time by 35%. The HTF flow rate also had a substantial influence on decreasing the charging time up to 21% when it was increased from 0.5 to 4 L/min.
- 2) The charging and discharging tests revealed that natural convection is the main heat transfer mechanism after the onset of melting during charging while conduction dominates the solidification of PCM during discharging. Hence, discharging tests took much longer to complete than the charging tests due to the poor conduction heat transfer within paraffin wax.
- 3) Switching the flow direction from upward to downward did not show a significant effect on either charging or discharging time. Running the tests at high flow rates resulted in uniform temperature along the heat exchanger coil. Therefore, the flow direction becomes insignificant for the current length of the helical coil heat exchanger.

- 4) Discharging tests that were run at high flow rates resulted in higher recovery efficiency.

5.2 Conclusions for NEPCM Study with Paraffin Wax

The second part of this study involved NEPCMs proposed as a solution to improving heat transfer for LHTESS. Several nanoparticles including MWCNTs, GNPs and Al_2O_3 were dispersed into paraffin wax for the enhancement of thermal properties. Characterization and stability studies were conducted to assess the feasibility of using NEPCM colloids in LHTESS. Some of the main findings from this study can be summarized as follows:

- 1) It seems that mechanical dispersion methods are not sufficient to achieve the long-term stability of paraffin wax-based NEPCM. Surfactants (sodium oleate and octadecylamine) along with stirring and sonication only maintained the stability of the paraffin wax-based NEPCM for limited time/cycles. These methods did not enhance long-term stability over multiple melting-solidification cycles.
- 2) The homogeneous and uniform dispersion of nanoparticles could not be maintained after sample preparation. The demonstrated stability problem explains the insignificant improvement in the thermal conductivity of NEPCMs found in the measurements.
- 3) DSC study of the NEPCMs showed anomalous latent heat capacity results without any trend. However, the presence of nanoparticles did have a negative effect on the supercooling issue.
- 4) Thermal boundary conditions during melting and solidification have important effects on nanoparticle stability. It was demonstrated that with heating from the

bottom of the material, natural convection in the melted MWCNT-wax NEPCM is favorable to sustain its stability, but only for limited thermal cycles. Settlement of nanoparticles started to happen during later solidification periods.

5.3 Recommendations for Future Work

Based on the results of the LHTESS study, alternative techniques of heat transfer enhancement need to be explored, particularly for discharging processes where conduction is the main heat transfer mechanism. Traditional enhancement methods with fins can be implemented; however, the position and geometry of fins should be carefully designed to improve heat transfer during both charging and discharging. Therefore, it is crucial that the optimal design improve the conduction heat transfer during discharging while not compromising the benefits of natural convection during charging.

Using NEPCMs in thermal energy storage applications could be a remedy to the existing poor heat transfer performance of PCMs. However, this method seems to be not feasible due to issues related to particle stability. Thus, a multidisciplinary approach is needed to continue to search for techniques to achieve the long-term real stability of NEPCMs. Many parameters are involved in the stability of a colloidal system. Multidisciplinary efforts are required to achieve a good understanding of these physical/chemical properties and to find the best combination or treatment for the long-term stability of the colloid.

Special porous media with microscale pores may enable overall uniformity and homogenous long-term dispersion of nanoparticles into PCMs. This could be a solution to the stability issue of NEPCMs. This technique is currently being investigated in our lab.

References

- Agyenim, F., Eames, P., & Smyth, M. (2009). A comparison of heat transfer enhancement in a medium temperature thermal energy storage heat exchanger using fins. *Solar Energy*, 83(9), 1509-1520.
- Akgün, M., Aydın, O., & Kaygusuz, K. (2008). Thermal energy storage performance of paraffin in a novel tube-in-shell system. *Applied Thermal Engineering*, 28(5), 405-413.
- Al-Abidi, A., Mat, S., Sopian, K., Sulaiman, Y., & Mohammad, A. (2016). Heat transfer enhancement for PCM thermal energy storage in triplex tube heat exchanger. *Heat Transfer Engineering*, 37(7-8), 705-712.
- Al-Shannaq, R., Kurdi, J., Al-Muhtaseb, S., Dickinson, M., & Farid, M. (2015). Supercooling elimination of phase change materials (PCMs) microcapsules. *Energy*, 87, 654-662.
- Angayarkanni, S. A., & Philip, J. (2015). Review on thermal properties of nanofluids: recent developments. *Advances in colloid and interface science*, 225, 146-176.
- Angayarkanni, S. A., & Philip, J. (2015). Thermal conductivity measurements in phase change materials under freezing in presence of nanoinclusions. *Journal of Applied Physics*, 118(9), 094306.
- Barreneche, C., Navarro, M. E., Cabeza, L. F., & Fernández, A. I. (2015). New database to select phase change materials: Chemical nature, properties, and applications. *Journal of Energy Storage*, 3, 18-24.
- Butt, H. J., Graf, K., & Kappl, M. (2003). *Physics and chemistry of interfaces*. John Wiley & Sons.
- Choi, S. U., & Eastman, J. A. (1995). *Enhancing thermal conductivity of fluids with nanoparticles* (No. ANL/MSD/CP--84938; CONF-951135--29). Argonne National Lab., IL (United States).

- Chu, S., & Majumdar, A. (2012). Opportunities and challenges for a sustainable energy future. *Nature*, 488(7411), 294-303.
- Cui, Y., Liu, C., Hu, S., & Yu, X. (2011). The experimental exploration of carbon nanofiber and carbon nanotube additives on thermal behavior of phase change materials. *Solar Energy Materials and Solar Cells*, 95(4), 1208-1212.
- Das, S. K., Choi, S. U., Yu, W., & Pradeep, T. (2007). *Nanofluids: science and technology*. John Wiley & Sons.
- Devices, D. (2011). KD2 Pro thermal properties analyzer operator's manual version 4. *Decagon Devices, Pullman, WA. KD2 Pro thermal properties analyzer operator's manual version,4*.
- Dincer, I., & Rosen, M. (2002). *Thermal energy storage: systems and applications*. John Wiley & Sons.
- Dinker, A., Agarwal, M., & Agarwal, G. D. (2017). Experimental assessment on thermal storage performance of beeswax in a helical tube embedded storage unit. *Applied Thermal Engineering*, 111, 358-368.
- Duan, X. L., Roul, J., Ryan, S., Hodder, S., & Stamp, J. (2016). Solar thermal energy storage with phase change material-heat exchanger design and heat transfer analysis. In *International Conference on Energy Engineering and Environmental Protection (EEEP 2016)*, Xiamen, China.
- Dutil, Y., Rousse, D. R., Salah, N. B., Lassue, S., & Zalewski, L. (2011). A review on phase-change materials: mathematical modeling and simulations. *Renewable and sustainable Energy reviews*, 15(1), 112-130.
- Elgafy, A., & Lafdi, K. (2005). Effect of carbon nanofiber additives on thermal behavior of phase change materials. *Carbon*, 43(15), 3067-3074.

- Ettouney, H. M., Alatiqi, I., Al-Sahali, M., & Al-Ali, S. A. (2004). Heat transfer enhancement by metal screens and metal spheres in phase change energy storage systems. *Renewable Energy*, 29(6), 841-860.
- Ettouney, H., El-Dessouky, H., & Al-Kandari, E. (2004). Heat transfer characteristics during melting and solidification of phase change energy storage process. *Industrial & engineering chemistry research*, 43(17), 5350-5357.
- Fan, L., & Khodadadi, J. M. (2011). Thermal conductivity enhancement of phase change materials for thermal energy storage: a review. *Renewable and Sustainable Energy Reviews*, 15(1), 24-46.
- Fan, L., & Khodadadi, J. M. (2011). Experimental verification of expedited freezing of nanoparticle-enhanced phase change materials (NEPCM). In *ASME conference proceedings* (Vol. 38921, pp. T10221-T10221).
- Fan, L. W., Fang, X., Wang, X., Zeng, Y., Xiao, Y. Q., Yu, Z. T., & Cen, K. F. (2013). Effects of various carbon nanofillers on the thermal conductivity and energy storage properties of paraffin-based nanocomposite phase change materials. *Applied Energy*, 110, 163-172.
- Fan, L. W., Zhu, Z. Q., Zeng, Y., Lu, Q., & Yu, Z. T. (2014). Heat transfer during melting of graphene-based composite phase change materials heated from below. *International Journal of Heat and Mass Transfer*, 79, 94-104.
- Fang, X., Fan, L. W., Ding, Q., Wang, X., Yao, X. L., Hou, J. F., & Cen, K. F. (2013). Increased thermal conductivity of eicosane-based composite phase change materials in the presence of graphene nanoplatelets. *Energy & Fuels*, 27(7), 4041-4047.
- Farid, M. M., Khudhair, A. M., Razack, S. A. K., & Al-Hallaj, S. (2004). A review on phase change energy storage: Materials and applications. *Energy conversion and management*, 45(9), 1597-1615.

- Filipponi, L., & Sutherland, D. (2013). Nanotechnologies: Principles, Applications, Implications and Hands-on Activities. *Publications Office of the European Union, Luxembourg*.
- Fleischer, A. S. (2015) *Thermal energy storage using phase change materials: Fundamentals and applications*. Springer.
- Ghadimi, A., Saidur, R., & Metselaar, H. S. C. (2011). A review of nanofluid stability properties and characterization in stationary conditions. *International Journal of Heat and Mass Transfer*, 54(17), 4051-4068.
- Ho, C. J., & Gao, J. Y. (2009). Preparation and thermophysical properties of nanoparticle-in-paraffin emulsion as phase change material. *International Communications in Heat and Mass Transfer*, 36(5), 467-470.
- Huang, M. J., Eames, P. C., McCormack, S., Griffiths, P., & Hewitt, N. J. (2011). Microencapsulated phase change slurries for thermal energy storage in a residential solar energy system. *Renewable Energy*, 36(11), 2932-2939.
- Huggins, R. (2015). *Energy storage: fundamentals, materials and applications*. Springer.
- Hyun, D. C., Levinson, N. S., Jeong, U., & Xia, Y. (2014). Emerging Applications of Phase-Change Materials (PCMs): Teaching an Old Dog New Tricks. *Angewandte Chemie International Edition*, 53(15), 3780-3795.
- Jesumathy, S., Udayakumar, M., & Suresh, S. (2012). Experimental study of enhanced heat transfer by addition of CuO nanoparticle. *Heat and Mass Transfer*, 48(6), 965-978.
- Kabbara, M., Groulx, D., & Joseph, A. (2014). Experimental study of a latent heat storage unit with a helical coil heat exchanger. In *CSME International Congress 2014, Toronto, Canada*.
- Kamalgharibi, M., Hormozi, F., Zamzamian, S. A. H., & Sarafraz, M. M. (2016). Experimental studies on the stability of CuO nanoparticles dispersed in different base

fluids: influence of stirring, sonication and surface-active agents. *Heat and Mass Transfer*, 52(1), 55-62.

Kenisarin, M., & Mahkamov, K. (2007). Solar energy storage using phase change materials. *Renewable and Sustainable Energy Reviews*, 11(9), 1913-1965.

Khodadadi, J. M., & Hosseinzadeh, S. F. (2007). Nanoparticle-enhanced phase change materials (NEPCM) with great potential for improved thermal energy storage. *International Communications in Heat and Mass Transfer*, 34(5), 534-543.

Khodadadi, J. M., Fan, L., & Babaei, H. (2013). Thermal conductivity enhancement of nanostructure-based colloidal suspensions utilized as phase change materials for thermal energy storage: A review. *Renewable and Sustainable Energy Reviews*, 24, 418-444.

Kibria, M. A., Anisur, M. R., Mahfuz, M. H., Saidur, R., & Metselaar, I. H. S. C. (2015). A review on thermophysical properties of nanoparticle dispersed phase change materials. *Energy Conversion and Management*, 95, 69-89.

Kim, S., & Drzal, L. T. (2009). High latent heat storage and high thermal conductive phase change materials using exfoliated graphite nanoplatelets. *Solar Energy Materials and Solar Cells*, 93(1), 136-142.

Korti, A. I. N., & Tlemsani, F. Z. (2016). Experimental investigation of latent heat storage in a coil in PCM storage unit. *Journal of Energy Storage*, 5, 177-186.

Kumaresan, V., Velraj, R., & Das, S. K. (2012). The effect of carbon nanotubes in enhancing the thermal transport properties of PCM during solidification. *Heat and Mass Transfer*, 48(8), 1345-1355.

Lokesh, S., Murugan, P., Sathishkumar, A., Kumaresan, V., & Velraj, R. (2015). Melting/solidification characteristics of paraffin based nanocomposite for thermal energy storage applications. *Thermal Science*, 21(6), 2517-2524.

Michaelides, E. E. S. (2014). *Nanofluidics: thermodynamic and transport properties*. Springer.

- Mehling, H., & Cabeza, L. F. (2007). Phase change materials and their basic properties. In *Thermal energy storage for sustainable energy consumption*, (pp. 257-277). Springer, Dordrecht.
- Mehrali, M., Latibari, S. T., Mehrali, M., Metselaar, H. S. C., & Silakhori, M. (2013). Shape-stabilized phase change materials with high thermal conductivity based on paraffin/graphene oxide composite. *Energy conversion and management*, 67, 275-282.
- Nabil, M., & Khodadadi, J. M. (2013). Experimental determination of temperature-dependent thermal conductivity of solid eicosane-based nanostructure-enhanced phase change materials. *International Journal of Heat and Mass Transfer*, 67, 301-310.
- Nomura, T., Tsubota, M., Oya, T., Okinaka, N., & Akiyama, T. (2013). Heat storage in direct-contact heat exchanger with phase change material. *Applied thermal engineering*, 50(1), 26-34.
- Nourani, M., Hamdami, N., Keramat, J., Moheb, A., & Shahedi, M. (2016). Thermal behavior of paraffin-nano- Al_2O_3 stabilized by sodium stearyl lactylate as a stable phase change material with high thermal conductivity. *Renewable Energy*, 88, 474-482.
- Nourani, M., Hamdami, N., Keramat, J., Moheb, A., & Shahedi, M. (2016). Preparation of a stable nanocomposite phase change material (NCPCM) using sodium stearyl lactylate (SSL) as the surfactant and evaluation of its stability using image analysis. *Renewable Energy*, 93, 404-411.
- Parsazadeh, M., & Duan, X. (2017). Numerical and statistical study on melting of nanoparticle enhanced phase change material in a shell-and-tube thermal energy storage system. *Applied Thermal Engineering*, 111, 950-960.
- Paul, G., Chopkar, M., Manna, I., & Das, P. K. (2010). Techniques for measuring the thermal conductivity of nanofluids: A review. *Renewable and Sustainable Energy Reviews*, 14(7), 1913-1924.
- Pielichowska, K., & Pielichowski, K. (2014). Phase change materials for thermal energy storage. *Progress in materials science*, 65, 67-123.

- Sabet, S. M., Mahfuz, H., Hashemi, J., Nezakat, M., & Szpunar, J. A. (2015). Effects of sonication energy on the dispersion of carbon nanotubes in a vinyl ester matrix and associated thermo-mechanical properties. *Journal of Materials Science*, 50(13), 4729-4740.
- Sari, A., & Karaipekli, A. (2007). Thermal conductivity and latent heat thermal energy storage characteristics of paraffin/expanded graphite composite as phase change material. *Applied Thermal Engineering*, 27(8), 1271-1277.
- Sari, A., & Kaygusuz, K. (2002). Thermal and heat transfer characteristics in a latent heat storage system using lauric acid. *Energy Conversion and Management*, 43(18), 2493-2507.
- Shaikh, S., Lafdi, K., & Hallinan, K. (2008). Carbon nanoadditives to enhance latent energy storage of phase change materials. *Journal of applied physics*, 103(9), 094302.
- Sharma, A., Tyagi, V. V., Chen, C. R., & Buddhi, D. (2009). Review on thermal energy storage with phase change materials and applications. *Renewable and Sustainable energy reviews*, 13(2), 318-345.
- Shaw, R. (2014). Dynamic Light Scattering Training.
- Shi, J. N., Ger, M. D., Liu, Y. M., Fan, Y. C., Wen, N. T., Lin, C. K., & Pu, N. W. (2013). Improving the thermal conductivity and shape-stabilization of phase change materials using nanographite additives. *Carbon*, 51, 365-372.
- Sundaram, P., Tiwari, R. K., & Kumar, S. (2016). Experimental Performance Study of Helical Coil Thermal Storage Unit Filled with PCM. *International Journal of ChemTech Research*, 9(7), 611-618.
- Tang, Q., Sun, J., Yu, S., & Wang, G. (2014). Improving thermal conductivity and decreasing supercooling of paraffin phase change materials by n-octadecylamine-functionalized multi-walled carbon nanotubes. *RSC Advances*, 4(69), 36584-36590.
- Tayssir, M., Eldemerdash, S. M., Sakr, R. Y., Elshamy, A. R., & Abdellatif, O. E. (2016). Experimental investigation of melting behavior of PCM by using coil heat source inside

cylindrical container. *Journal of Electrical Systems and Information Technology*, 4(1), 18-33.

Teng, T. P., & Yu, C. C. (2012). Characteristics of phase-change materials containing oxide nano-additives for thermal storage. *Nanoscale research letters*, 7(1), 611.

Ukrainczyk, N., Kurajica, S., & Šipušić, J. (2010). Thermophysical comparison of five commercial paraffin waxes as latent heat storage materials. *Chemical and biochemical engineering quarterly*, 24(2), 129-137.

Ultrasonics, B. (2001). Digital Sonifier Models 250 & 450 User's Manual, Branson Ultrasonics Corporation.

Wang, J., Xie, H., & Xin, Z. (2009). Thermal properties of paraffin based composites containing multi-walled carbon nanotubes. *Thermochimica Acta*, 488(1), 39-42.

Wang, J., Xie, H., Li, Y., & Xin, Z. (2010). PW based phase change nanocomposites containing γ -Al₂O₃. *Journal of Thermal Analysis and Calorimetry*, 102(2), 709-713.

Warzoha, R. J., & Fleischer, A. S. (2014). Improved heat recovery from paraffin-based phase change materials due to the presence of percolating graphene networks. *International Journal of Heat and Mass Transfer*, 79, 314-323.

Weinstein, R. D., Kopec, T. C., Fleischer, A. S., D'Addio, E., & Bessel, C. A. (2008). The experimental exploration of embedding phase change materials with graphite nanofibers for the thermal management of electronics. *Journal of Heat Transfer*, 130(4), 042405.

Wu, S., Zhu, D., Zhang, X., & Huang, J. (2010). Preparation and melting/freezing characteristics of Cu/paraffin nanofluid as phase-change material (PCM). *Energy & fuels*, 24(3), 1894-1898.

Wu, S. Y., Tong, X., Nie, C. D., Peng, D. Q., Gong, S. G., & Wang, Z. Q. (2016). The effects of various carbon nanofillers on the thermal properties of paraffin for energy storage applications. *Journal of Thermal Analysis and Calorimetry*, 124(1), 181-188.

- Xu, B., Li, P., & Chan, C. (2015). Application of phase change materials for thermal energy storage in concentrated solar thermal power plants: A review to recent developments. *Applied Energy*, 160, 286-307.
- Yang, Y., Luo, J., Song, G., Liu, Y., & Tang, G. (2014). The experimental exploration of nano-Si₃N₄/paraffin on thermal behavior of phase change materials. *Thermochimica Acta*, 597, 101-106.
- Yang, X., Xiong, T., Dong, J. L., Li, W. X., & Wang, Y. (2017). Investigation of the dynamic melting process in a thermal energy storage unit using a helical coil heat exchanger. *Energies*, 10(8), 1129.
- Yu, Z. T., Fang, X., Fan, L. W., Wang, X., Xiao, Y. Q., Zeng, Y., & Cen, K. F. (2013). Increased thermal conductivity of liquid paraffin-based suspensions in the presence of carbon nano-additives of various sizes and shapes. *Carbon*, 53, 277-285.
- Zhang, S., Wu, J. Y., Tse, C. T., & Niu, J. (2012). Effective dispersion of multi-wall carbon nano-tubes in hexadecane through physiochemical modification and decrease of supercooling. *Solar Energy Materials and Solar Cells*, 96, 124-130.
- Zhang, S., Zhang, L., Yang, X., Yu, X., Duan, F., Jin, L., & Meng, X. (2017). Experimental Investigation of a Spiral Tube Embedded Latent Thermal Energy Storage Tank Using Paraffin as PCM. *Energy Procedia*, 105, 4543-4548.
- Zeng, Y., Fan, L. W., Xiao, Y. Q., Yu, Z. T., & Cen, K. F. (2013). An experimental investigation of melting of nanoparticle-enhanced phase change materials (NePCMs) in a bottom-heated vertical cylindrical cavity. *International Journal of Heat and Mass Transfer*, 66, 111-117.
- Zhou, D., & Zhao, C. Y. (2011). Experimental investigations on heat transfer in phase change materials (PCMs) embedded in porous materials. *Applied Thermal Engineering*, 31(5), 970-977.